A UNITED STATES DEPARTMENT OF COMMERCE PUBLICATION

NBS TECHNICAL NOTE 594-1

Optical Radiation Measurements:

Fundamental Principles of Absolute Radiometry and the Philosophy of This NBS Program (1968 to 1971)

U.S. DEPARTMENT OF COMMERCE
National Bureau of Standards

NATIONAL BUREAU OF STANDARDS

The National Bureau of Standards[1] was established by an act of Congress March 3, 1901. The Bureau's overall goal is to strengthen and advance the Nation's science and technology and facilitate their effective application for public benefit. To this end, the Bureau conducts research and provides: (1) a basis for the Nation's physical measurement system, (2) scientific and technological services for industry and government, (3) a technical basis for equity in trade, and (4) technical services to promote public safety. The Bureau consists of the Institute for Basic Standards, the Institute for Materials Research, the Institute for Applied Technology, the Center for Computer Sciences and Technology, and the Office for Information Programs.

THE INSTITUTE FOR BASIC STANDARDS provides the central basis within the United States of a complete and consistent system of physical measurement; coordinates that system with measurement systems of other nations; and furnishes essential services leading to accurate and uniform physical measurements throughout the Nation's scientific community, industry, and commerce. The Institute consists of a Center for Radiation Research, an Office of Measurement Services and the following divisions:

Applied Mathematics—Electricity—Heat—Mechanics—Optical Physics—Linac Radiation[2]—Nuclear Radiation[2]—Applied Radiation[2]—Quantum Electronics[3]—Electromagnetics[3]—Time and Frequency[3]—Laboratory Astrophysics[3]—Cryogenics[3].

THE INSTITUTE FOR MATERIALS RESEARCH conducts materials research leading to improved methods of measurement, standards, and data on the properties of well-characterized materials needed by industry, commerce, educational institutions, and Government; provides advisory and research services to other Government agencies; and develops, produces, and distributes standard reference materials. The Institute consists of the Office of Standard Reference Materials and the following divisions:

Analytical Chemistry—Polymers—Metallurgy—Inorganic Materials—Reactor Radiation—Physical Chemistry.

THE INSTITUTE FOR APPLIED TECHNOLOGY provides technical services to promote the use of available technology and to facilitate technological innovation in industry and Government; cooperates with public and private organizations leading to the development of technological standards (including mandatory safety standards), codes and methods of test; and provides technical advice and services to Government agencies upon request. The Institute also monitors NBS engineering standards activities and provides liaison between NBS and national and international engineering standards bodies. The Institute consists of the following divisions and offices:

Engineering Standards Services—Weights and Measures—Invention and Innovation—Product Evaluation Technology—Building Research—Electronic Technology—Technical Analysis—Measurement Engineering—Office of Fire Programs.

THE CENTER FOR COMPUTER SCIENCES AND TECHNOLOGY conducts research and provides technical services designed to aid Government agencies in improving cost effectiveness in the conduct of their programs through the selection, acquisition, and effective utilization of automatic data processing equipment; and serves as the principal focus within the executive branch for the development of Federal standards for automatic data processing equipment, techniques, and computer languages. The Center consists of the following offices and divisions:

Information Processing Standards—Computer Information—Computer Services—Systems Development—Information Processing Technology.

THE OFFICE FOR INFORMATION PROGRAMS promotes optimum dissemination and accessibility of scientific information generated within NBS and other agencies of the Federal Government; promotes the development of the National Standard Reference Data System and a system of information analysis centers dealing with the broader aspects of the National Measurement System; provides appropriate services to ensure that the NBS staff has optimum accessibility to the scientific information of the world, and directs the public information activities of the Bureau. The Office consists of the following organizational units:

Office of Standard Reference Data—Office of Technical Information and Publications—Library—Office of International Relations.

---

[1] Headquarters and Laboratories at Gaithersburg, Maryland, unless otherwise noted; mailing address Washington, D.C. 20234.
[2] Part of the Center for Radiation Research.
[3] Located at Boulder, Colorado 80302.

Optical Radiation Measurements:

Fundamental Principles of Absolute Radiometry and the Philosophy of This NBS Program (1968 to 1971)

Jon Geist

Heat Division
Institute for Basic Standards
National Bureau of Standards
Washington, D.C. 20234

Work supported in part by the National Aeronautics and Space Administration under Contract C-41584-B.

U.S. DEPARTMENT OF COMMERCE, Peter G. Peterson, *Secretary*
NATIONAL BUREAU OF STANDARDS, Lawrence M. Kushner, *Acting Director,*

Issued June 1972

National Bureau of Standards Technical Note 594-1

Nat. Bur. Stand. (U.S.), Tech. Note 594-1, 59 pages (June 1972)

CODEN: NBTNAE

For sale by the Superintendent of Documents, U.S. Government Printing Office, Washington, D.C. 20402
(Order by SD Catalog No. C13.46:594-1). Price 60 cents.

FORM NBS-114A (1-71)

U.S. DEPT. OF COMM. BIBLIOGRAPHIC DATA SHEET	1. PUBLICATION OR REPORT NO. NBS TN-594-1	2. Gov't Accession No.	3. Recipient's Accession No.

4. TITLE AND SUBTITLE

OPTICAL RADIATION MEASUREMENTS:
Fundamental Principles of Absolute Radiometry and the Philosophy of This NBS Program (1968 to 1971)

5. Publication Date: June 1972

6. Performing Organization Code

7. AUTHOR(S): Jon Geist

8. Performing Organization

9. PERFORMING ORGANIZATION NAME AND ADDRESS

NATIONAL BUREAU OF STANDARDS
DEPARTMENT OF COMMERCE
WASHINGTON, D.C. 20234

10. Project/Task/Work Unit No.

11. Contract/Grant No.: C-41584-B

12. Sponsoring Organization Name and Address

Work supported in part by the National Aeronautics and Space Administration under Contract C-41584-B.

13. Type of Report & Period Covered: Final

14. Sponsoring Agency Code

15. SUPPLEMENTARY NOTES

16. ABSTRACT (A 200-word or less factual summary of most significant information. If document includes a significant bibliography or literature survey, mention it here.)

The philosophy of the present NBS program in realizing a scale of total irradiance with electrically calibrated (absolute) detectors, a theoretical analysis of the sources of error in such a scale realization, a description of the electrically calibrated detector developed from 1968 to 1971, and participation in the Third International Pyrheliometer Comparison are presented.

17. KEY WORDS (Alphabetical order, separated by semicolons)

Absolute detector radiometry; electrically calibrated detectors; International Pyrheliometric Scale; irradiance; radiometry.

18. AVAILABILITY STATEMENT

[x] UNLIMITED.

[ ] FOR OFFICIAL DISTRIBUTION. DO NOT RELEASE TO NTIS.

19. SECURITY CLASS (THIS REPORT): UNCLASSIFIED

21. NO. OF PAGES: 59

20. SECURITY CLASS (THIS PAGE): UNCLASSIFIED

22. Price: 60 cents

USCOMM-DC 66244-P71

C-2

Preface

This is the first issue of a series of Technical Notes entitled OPTICAL RADIATION MEASUREMENTS. The series will consist primarily of reports of progress in or details of research conducted in radiometry and photometry in the Optical Radiation Section of the Heat Division and will appear about every six weeks.

The level of presentation in OPTICAL RADIATION MEASUREMENTS will be directed at a general technical audience. The equivalent of an undergraduate degree in engineering or physics plus familiarity with the basic concepts of radiometry and photometry [e.g., G. Bauer, Measurement of Optical Radiations (Focal Press, London, New York, 1965)] should be sufficient for understanding the vast majority of material in this series. Occasionally a more specialized background will be required such as a few of the mathematical techniques required in this issue. Even in such instances, a careful reading of the assumptions, approximations and final conclusions should permit the non-specialist to understand the gist of the argument if not the details.

At times, certain commercial materials and equipment will be identified in this series in order to adequately specify the experimental procedure. In no case does such identification imply recommendation or endorsement by the National Bureau of Standards, nor does it imply that the material or equipment identified is necessarily the best available for the purpose.

Any suggestions readers may have to improve the utility of this series are welcome.

Henry J. Kostkowski, Chief,
Optical Radiation Section
National Bureau of Standards

Contents

Fundamental Principles of Absolute Radiometry and The Philosophy of this NBS Program (1968 to 1971)

Jon Geist

The philosophy of the present NBS program in realizing a scale of total irradiance with electrically calibrated (absolute) detectors, a theoretical analysis of the sources of error in such a scale realization, a description of the electrically calibrated detector developed from 1968 to 1971, and participation in the Third International Pyrheliometer Comparison are presented.

Key words: Absolute detector radiometry; electrically calibrated detectors; International Pyrheliometric Scale; irradiance; radiometry.

1. Introduction

This report describes work performed on a program to develop an electrically calibrated detector (also called absolute radiometer, absolute detector, and electrically calibrated radiometer) that could be used to realize, maintain, and transfer a scale of total irradiance. The program included a comprehensive investigation of the theoretical basis of absolute detector radiometry, as well as the design and construction of a number of detectors. This part of the final report covers the period from the inception of the program through the end of 1970, and concentrates on two areas. Sections 2, 3, and 4 of this report describe all of the theoretical work carried out under the program with the exception of work reported in a paper,"A New Type of Boundary Value Coupling for Second Order Sturm-Liouville Systems", J. Res. Nat. Bur. Stand. (U.S.), B, 75B (Math. Sci.), Nos. 3 and 4, 121-132 (July-Dec. 1971). Section 5 describes one of the detectors designed and constructed under this program and its participation in the Third International Pyrheliometer Comparisons in Davos, Switzerland in September of 1970.

2. Definition and Historical Review of Absolute Radiometry

The measurement of certain radiometric quantities such as reflectance and emittance does not require a knowledge of the power levels of the fluxes which are used in the measurement. Only the ratios of the fluxes are important. Thus we could classify such measurements as relative radiometry. The rest of radiometry is concerned with power levels through the quantities, radiance, irradiance, and intensity.

How are scales of these radiometric quantities to be realized? One way is to compare the flux to be measured with the flux emitted by a blackbody, either directly, or using a standard which in turn has been calibrated by comparison with a blackbody. Here the ultimate accuracy with which the radiometric scales can be realized will depend upon the accuracy with which the thermodynamic temperature scale can be realized, and the validity of the Stefan-Boltzmann and Planck laws of blackbody radiation. Any other method of realizing radiometric scales can be classified as absolute radiometry. Of course this is not a particularly good name, since it is not at all descriptive of the activity to which it is applied. However, this name does have historical precedent. I think it arose in reference to absolute electrical measurements. At any rate, it is important to understand that it is no more absolute to realize a radiometric scale through absolute radiometry, than to realize it by reference to blackbody radiation.

By far the most common absolute radiometric measurements are made with thermal detectors (power meters) which have an electric heater built into their receivers. Here the power carried by the radiant flux which is to be measured is compared with the power carried by an electrical current. This, in turn, can be determined by relatively straightforward voltage and current measurements. In this case the ultimate accuracy with which the radiometric scales can be realized will depend upon the accuracy with which the (absolute) voltage and current scales can be realized.

If all is well with the laws of physics, and the realizations of the thermodynamic temperature scale and the absolute voltage and current scales, then a blackbody radiometric scale should be consistent with an absolute radiometric scale of the same quantity, to within

the combined estimated uncertainties of the scales, provided these estimates are realistic.

The actual situation as to the consistency of radiometric scales derived from blackbody and absolute radiometric measurements is uncertain. A large amount of work has been done, most of it quite early, which has shown a discrepancy of at least 1/2% between the measured value of the Stefan-Boltzmann constant, σ, and its theoretical value as calculated from atomic constants. It is interesting that in 1929 the errors in the measured values of Planck's constant, h, and the Boltzmann constant, k, were of just the right magnitude and direction (about 1% each) to make the value of σ calculated by Birge [1][1] using these values agree to better than .1% with the value that had been measured over ten years earlier by Coblentz [2]. Later measurements of σ were consistently higher than Coblentz's value [1,3] so that by the time the errors in h and k were discovered, no redeterminations of σ were attempted. After a 24-year period between 1933 and 1957 when no measurements of σ were reported, Eppley and Karoli [4] reported a value higher than that of Coblentz, but they chose not to discuss the discrepancy between their value and the theoretical value. In 1962 Gillham attempted to measure σ but discovered evidence of systematic errors in his results and did not publish them. However, his result, which was a little higher than that of Coblentz, was reported in the literature by Stair [5] with a reference to a personal communication from Gillham. To complete the picture, it must be noted that most scientists who were aware of the lingering discrepancy between the measured and theoretical values of σ, had concluded that some source of error must have been overlooked by all of the investigators [6].

3. Fundamental Considerations in the Present Program

As mentioned in the last section, the consensus of opinion is that the discrepancy between the theoretical and experimental values of σ is due to experimental errors in the absolute radiometric measurements. Consequently any attempt to resolve this issue must be carried out in an extremely careful manner, so that whatever the outcome, no doubts will persist as to the experimental technique. Furthermore, any results from absolute radiometric techniques must be viewed with suspicion until this issue is resolved. In view of this fact we approach this problem from as fundamental a viewpoint as possible. First, we analyze the fundamental concepts of error in the measurement process.

3.1 Error in the Measurement Process

Some people would reserve the word error for the difference between the result of a measurement and the "true" values of the measured quantity. However, in order to describe the measurement process in detail, the word error is sometimes used in a different sense. This sense is best described in terms of the measurement process itself. Here one starts with a physical principle, a law of physics, which describes a particular phenomena. An instrument whose behavior is governed primarily by this physical law, is designed and used to measure the physical quantity described by the physical law. Any deviations of the instrument's behavior from the ideal behavior predicted by the law are due to the fact that the instrument must obey all of the other laws of physics, and can be called an error. In this view, every other law of physics is a possible source of error in the instrument. If no corrections are made for any of the instrument's departures from the ideal behavior predicted by the physical law, the difference between the two possible meanings of the word error is not important. However, if a correction is applied to compensate for a particular error, the different uses of the word error become quite significant. For want of a better word, we will use the word error in the second sense[2].

There are at least two different philosophies with respect to errors which can govern the design of scientific instruments. Under the first of these philosophies, we would strive to minimize each of the errors which affect the instrument. The actual magnitudes of the errors may be subject to considerable uncertainty, but at least they are as small as possible within the design constraints imposed by other factors. Under the second philosophy, we no longer strive to minimize each error. Instead we try to minimize the uncertainty with which

---

[1]Figures in brackets indicate the literature references at the end of this paper.

[2]The semantic problem is further complicated in that as long as we do not make corrections for these errors, we call them errors, but as soon as we make a correction for them, we call them corrections, or else we don't refer to them.

each error is known. This can be accomplished by designing the instrument in such a way that the actual value of each error can be precisely and accurately determined in a definitive measurement. Of course, it is possible that an instrument design which permits some particular error to be measured, will be such that this error is much larger than its minimum achievable value. However, this is not an unsatisfactory situation. While the error itself is not a minimum, the uncertainty with which it is known is a minimum. This is certainly the more desirable situation. So much so, in fact, that at this point, one might wonder why any instrument would be designed under the first philosophy. However, the whole picture has not been presented yet.

It is obviously more difficult to use an instrument which has been designed under the second philosophy, than one which has been designed for the same purpose under the first philosophy because the measurements of the errors have to be conducted in addition to the measurements which are associated with the normal use of the instrument. Furthermore, if the measurement process is examined in detail, it usually turns out that the measurements of the errors are more difficult and time consuming than the measurements for which the instrument was designed. As a result, most instruments are designed (consciously or not) according to the first philosophy for some sources of error and the second philosophy for other sources of error. Those errors which are easy to measure are measured, and those errors which are difficult to measure are minimized.

A popular compromise of the two philosophies must also be considered. One might design an instrument in such a way as to minimize the errors, and then attempt to calculate their actual magnitude from property data for the materials from which the instrument was constructed. The second philosophy is still represented, since measurements have been performed to determine the magnitude of each error. However, they were not performed on the instrument itself, but on materials which are similar to those incorporated into the instrument. The advantages of this approach are usually illusory. It often happens that no reliable uncertainties can be associated with the property data that is available in the literature and hence no reliable uncertainty can be associated with an estimate of error which is based on this data. Secondly, it is often the case that the samples of the material upon which the property measurements were made are not representative of the samples of the material which were incorporated into the instrument. Again no reliable uncertainties can be obtained.

We turn our attention now to a practical example of the two philosophies. In sophisticated measurement systems, it is possible to distinguish two different types of instruments which roughly correspond to the two philosophies with respect to error. Here we differentiate between instruments which are used to realize a scale of a physical quantity and those to which this scale is transferred and which are used to maintain and transfer the scale but which are not used to realize it. The more the second philosophy governs the design of instruments which are used to realize a scale, the less uncertain the scale will be. However, instruments which are not used to realize scales, but only to transfer scales, are often best designed under the first philosophy. In effect, the transfer of the scale from the instrument which has realized it to the secondary instrument is a measurement of the sum of all of the errors associated with the secondary instrument. The uncertainty in the knowledge of the sum of all the errors in the secondary instrument is just the combined uncertainty in the sum of all of the errors in the instrument which was used to realize the scale, and the uncertainty in the transfer of the scale. The advantage of minimizing the errors in this type of instrument is that under these conditions the minimum number of variations in experimental conditions need be performed in the scale transfer. The reason for this is that interpolation between various experimental conditions will be more accurate when the errors are small.

3.2 The Principle of Operation of an Absolute Radiometer

The purpose of the absolute radiometer developed on this project is to accurately realize a scale of irradiance which can be made available to the scientific and technical community. Consequently the second philosophy with respect to error was chosen as the primary design philosophy for this instrument. The past difficulties associated with the experimental determinations of the Stefan-Boltzmann constant imposed a total commitment to this design philosophy.

In this section we first state the Principle of Operation of an Absolute Radiometer.

By examining this principle we then determine the various sources of error in all absolute radiometers. Then we can attempt to design the instrument so that all of the errors arising from all of these sources can be measured in definitive experiments. The actual instrument design which was finally adopted will be described in section 5.

The Principle of Operation of an Absolute Radiometer can be simply stated in the following manner:

If a) irradiation of the receiver with radiant power and dissipation in the receiver of electrical power result in the same temperature distribution throughout the entire radiometer, then b) the amount of radiant power absorbed by the receiver must equal the amount of electrical power absorbed by the receiver.

This principle follows from conservation of energy and a few laws of heat transfer. As might be expected, other physical laws prevent any absolute radiometer from behaving in such a way that the principle can be realized. It is impossible to design a radiometer in which the temperature distributions under radiant and electrical heating are identical. Also, it is impossible to measure the exact temperature distribution within the radiometer. What is usually measured is a voltage which is proportional to some weighted average temperature difference between the receiver of the radiometer and its thermal environment, (plus a random noise voltage). We will restrict the following discussion to such radiometers. If we assume this much, it is possible to isolate the sources of error which affect this type of radiometer. Then we can determine the type of measurements which must be conducted in order to obtain corrections for the sources of error which have been isolated.

3.3 Sources of Error in Absolute Radiometers

In this section we examine in a detailed but qualitative manner the sources of error associated with absolute radiometers. Figure 1 is a schematic diagram of a "general" absolute radiometer from which the various sources of error can be obtained by applying the Principle of Operation. First of all, in order to employ the principle we must measure the voltage across the thermopile and the voltage across and the current in the heater during the periods of electrical and radiant heating of the receiver. And if we wish to realize a scale of irradiance, we must also measure the area of the aperture. Thus any sources of error in these measurements are sources of error which must be accounted for in the absolute radiometer. However, there are more subtle sources of error affecting absolute radiometers than these.

Referring to figure 1, first consider the heat transfer taking place within the radiometer during a period of electrical heating. The electrical current generates heat in the heater leads as well as in the heater itself. The resulting temperature distribution within the radiometer is such that some of the heat generated in the heater is conducted to the receiver and some is carried to the thermal environment of the receiver by radiation and convection. The heat conducted to the receiver is distributed throughout the receiver and the high absorptance coating of the receiver (its distribution being governed by the equations of heat transfer) and is ultimately carried to the thermal environment of the receiver by conduction down the thermopile legs and the heater leads, and by convection and radiation from all of the surfaces of the receiver, including the high absorptance coating, the thermopile legs, and the heater leads. Likewise, some of the heat which is generated in the heater leads is carried to the thermal environment of the receiver by conduction down the leads and by convection and radiation from the surfaces of the leads. While none of the heat generated in the leads is conducted to the receiver, the heat generation in the leads causes the temperature distribution within the radiometer to be different from that which would be obtained with no lead heating. Thus two of the sources of error which prevent an absolute radiometer from rigorously fulfilling the Principle of Operation are (1) not all of the power generated in the heater is absorbed by the receiver, and (2) the heat generated in the heater leads modifies the temperature distribution within the radiometer.

Now let us consider the heat transfer taking place within the radiometer during a period of radiant heating. Electromagnetic radiation (indicated by the arrows in figure 1) is incident on the aperture and on the thermal environment of the receiver. The portion of the incident flux which passes through the aperture is incident on the high absorptance coating of the receiver. Some of this flux is reflected off of the coating, the rest is absorbed in

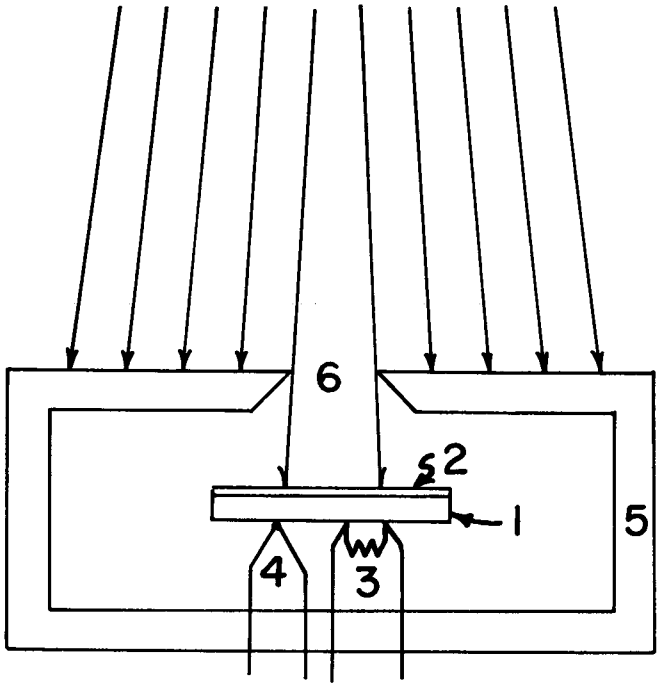

Figure 1. A "general" absolute radiometer. 1 - receiver disk, 2 - high absorptance coating of receiver disk, 3 - heater, 4 - thermocouple, 5 - thermal environment of receiver, 6 - aperture. The word receiver usually applies to 1, 2, and 3.

the coating causing it to have a different temperature distribution than during a period of electrical heating. Some of the flux absorbed by the high absorptance coating is carried to the thermal environment by convection and radiation, and the rest is conducted to the receiver. From this point on it suffers a fate similar to that suffered by the heat generated electrically, but the temperature distribution in the receiver will be somewhat different since the power enters the receiver from a different location. In a similar manner, a portion of the flux incident on the thermal environment of the receiver is absorbed by the thermal environment causing it to have a different temperature distribution than that which it has during a period of electrical heating. Thus, three more sources of error are (1) not all of the flux incident on the high absorptance coating is absorbed, (2) the flux incident on the thermal environment modifies the temperature distribution within the radiometer, and (3) the temperature distributions within the high absorptance coating and the receiver are different during periods of electrical and radiant heating.

The above described sources of error can be divided into two categories:

I. Errors associated with the measurement of physical quantities
   - voltage across thermopile
   - voltage across heater
   - current in heater
   - area of aperture

II. Errors associated with getting the power into the receiver
   - not all of the electrical power generated in the heater is absorbed by the receiver.

- not all of the radiant power incident on the high absorptance coating is absorbed by it
- power generated in the heater leads modifies the temperature distribution within the radiometer
- flux incident on the thermal environment of the receiver modifies the temperature distribution within the radiometer
- the temperature distribution in the receiver and high absorptance coating during radiant heating is different from that during electrical heating.

Having isolated the sources of error, we must next design definitive experiments in which corrections for the various errors can be measured and which will provide reliable uncertainties associated with each correction. This problem will be discussed in the following sections. However, before doing so it is useful to consider the distinction between the two different categories into which we have divided the sources of error. Presumably, the instruments which we use to measure the physical quantities listed under the first category were designed according to the first design philosophy described in section 3.1, that is, to minimize the various errors affecting the instrument. Furthermore, it is reasonable to assume that each of them has been calibrated against some other instrument which was designed according to the second philosophy and which was used to realize a scale of the physical quantity in question. In this case the cumulative correction and associated uncertainty describing the ability of each of these instruments to transfer the scale it is maintaining is well known and well documented, for instance, in a calibration report. Consequently, we will assume that the sources of error in the first category are known and we will restrict our efforts in the following sections to studying the problems associated with measuring the correction factors which apply to the sources of error in the second category.

We conclude this section by pointing out that while it is possible to calculate these corrections using published values for material properties, the problems which were mentioned in section 3.1 in regard to this approach are especially severe here. The estimates of uncertainty which accompany thermal data, particularly thermal-radiative data are usually unreliable, and it is questionable whether the samples on which the published measurements were made are representative of the same material incorporated into the absolute radiometer. Thus the uncertainties associated with corrections obtained in this manner cannot be considered reliable. For emphasis the general conclusion reached earlier in this paper will be restated. Any detector that is going to be used to realize a scale of total irradiance must be constructed in such a way that all of the measurements which are necessary to obtain the corrections for the errors in the second category can be made on that detector. This must be the primary design consideration.

4. Techniques for Measuring Corrections for the Various Errors Affecting Absolute Radiometers

In the following sections we will describe experiments by which corrections for the various errors identified in the last section can be measured. In order to understand these experiments, and in fact, in order to convincingly demonstrate that these experiments do indeed measure the quantities of interest, we will need to look more deeply and in a quantitative manner into these various errors. First we note that all of the experiments which we will describe are based on the following principle which depends upon the Principle of Operation of an Absolute Radiometer. Each of the sources of error causes a different temperature distribution within the radiometer and this different temperature distribution produces a different thermopile voltage than that which would be produced in the absence of that particular source of error. In other words, the different thermopile voltage is how the error manifests itself.

Now suppose that we can devise an experiment in which one of the sources of error can be turned on and off while all other conditions within the radiometer are maintained identical to those existing during some particular irradiance measurement. Then the difference between the thermopile voltages existing when the source of error is turned on and off will be the error produced when the conditions of the particular irradiance measurement exist within the radiometer. The negative of this difference is, therefore, the exact voltage

correction to be applied to the radiometer output in order to correct for that particular source of error during the actual irradiance measurement.

We will attempt to devise such an experiment for each of the sources of error described earlier. However, it is clear that we will not be able to make the conditions existing within the radiometer during each of these experiments identical to those existing during some specified irradiance measurement. But we will be able to make them similar in each case, and we will be able to establish limits on the systematic error introduced by our failure to keep them identical.

In the following section, we will investigate from a theoretical point of view, the responsivity as a function of position over the surface of a simplified model of a receiver. This model most closely resembles the radiometers which have evolved at the National Bureau of Standards during the period covered by this report. However, significant conclusions about the radiometers of Guild [7], Gillham [8], Blevin and Brown [9], Bischoff [10] and Kendall and Berdahl [11] will be inferred from the results of this analysis. Sections 4.2 and 4.3 will describe correction factor experiments whose design is based on the results of this analysis. Finally, section 4.4 will describe the experiments needed to determine the rest of the correction factors for the sources of error identified in section 3.3.

4.1 The Theory of the Responsivity of the Receiver to Power Inputs from Various Locations

In this section we derive an equation which is simple enough to be solved analytically, but which is at the same time general enough to accurately describe the important characteristics of the steady state operation of the receiver. The analytic techniques that we will use include delta functions, the solution of inhomogeneous partial differential equations with Greens functions, and special functions. These techniques will not be developed in detail since they can be found in numerous mathematical texts.

An exploded view of the specific receiver configuration to be analyzed is shown in figure 2. The radiant power is incident on the top of surface 1, the high absorptance coating. It must be conducted through this coating and the insulating substrate before reaching the receiver disk which acts as a thermal averaging device.

We will start with the equation [12] which describes the temperature distribution, $T(\rho, \phi, z)$, in the receiver disk. It is

$$k_d \nabla^2 T = k_d \left[\frac{1}{\rho} \frac{\partial}{\partial \rho} \left(\rho \frac{\partial T}{\partial \rho} \right) + \frac{1}{\rho^2} \frac{\partial^2 T}{\partial \phi^2} + \frac{\partial^2 T}{\partial z^2} \right] = 0 , \tag{1}$$

where k_d is the thermal conductivity of the material in the disk. The coordinate system is shown in figure 3. Next we obtain a simpler equation for the average temperature distribution along the height of the disk, by integrating eq. (1) with respect to z. The average temperature, $U(\rho, \phi)$, is given by

$$U = \frac{1}{z_d} \int_0^{z_d} T(\rho, \phi, z)\, dz. \tag{2}$$

The result of this procedure is the equation,

$$z_d k_d \left[\frac{1}{\rho} \frac{\partial}{\partial \rho} \left(\rho \frac{\partial U}{\partial \rho} \right) + \frac{1}{\rho^2} \frac{\partial^2 U}{\partial \phi^2} \right] + k_d \left[\left. \frac{\partial T}{\partial z} \right|_{z_d} - \left. \frac{\partial T}{\partial z} \right|_0 \right] = 0 . \tag{3}$$

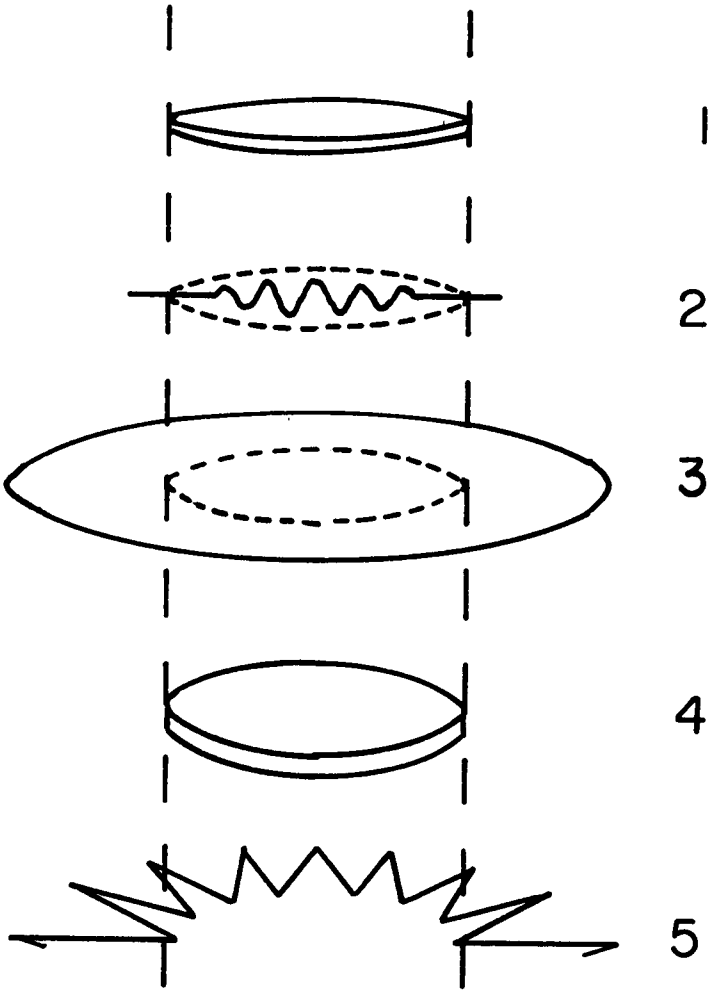

Figure 2. A specific receiver configuration for theoretical analysis. 1 - high absorptance coating, 2 - heater, 3 - electrically insulating heater substrate, 4 - high thermal conductivity receiver disk, 5 - radial thermopile to measure average temperature difference between edge of receiver disk and thermal environment.

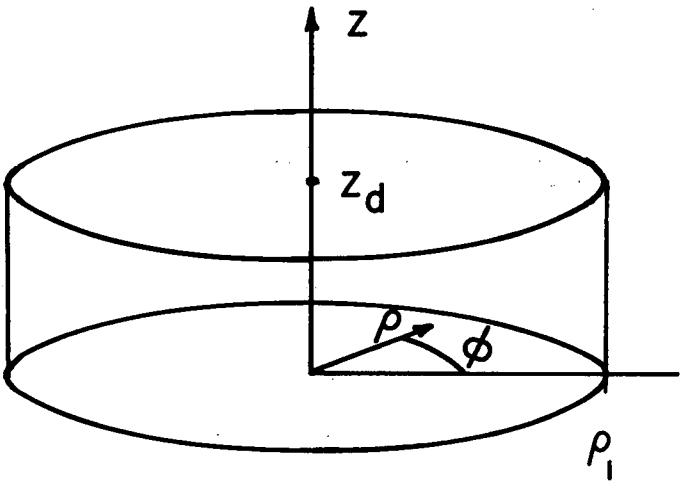

Figure 3. Coordinate system used to analyze the temperature distribution in the receiver disk.

Now we assume that heat flows only in the z direction through the substrate and high absorptance coating, or at least that any other heat flow is negligible. This is a good assumption as long as the substrate and high absorptance coating are thin compared to their own radii and the dimensions of the receiver disk, and as long as their thermal conductivity is much less than that of the receiver disk. We further assume that the variation in temperature in the z direction in the receiver disk is negligible in comparison with the difference in temperature between the disk and its environment. In other words, $T(\rho, \phi, z)$ is approximated by $U(\rho, \phi)$. This is a very good approximation because any variation in temperature in the z direction which does exist is small. Moreover, it is virtually independent of the mode of heating and therefore will cancel out when electrical and radiant heating are compared. Applying the law of conservation of energy and these two assumptions to the upper and lower surfaces of the receiver disk yields the following boundary conditions:

$$k_d \left.\frac{\partial T}{\partial z}\right|_0 = h_0(U - T_0) \quad , \tag{4}$$

and

$$k_d \left.\frac{\partial T}{\partial z}\right|_{z_d} = -h_c(U - \Delta T - T_0) + E \quad , \tag{5}$$

where

$$\Delta T = U - T_c \quad . \tag{6}$$

Here, h_0 is the heat transfer coefficient of the bottom surface of the receiver and h_c is the heat transfer coefficient of the top surface of the high absorptance coating (surface 1 in figure 2). They are measures of the rate at which power is lost by these surfaces per unit area and temperature difference between the surfaces and their environment [13]. The product of a heat transfer coefficient and an area is a thermal conductance which is the reciprocal of the thermal resistance. T_0 is the temperature of the environment, and T_c is the temperature of the top surface of the high absorptance coating, at the point, (ρ, ϕ). Finally, $E = E(\rho, \phi)$ is the power density input to the detector, an arbitrary function of position. Now we must examine the cases of radiant and electrical heating separately.

The case of radiant heating: let ΔT_c and ΔT_s denote the temperature differences across the high absorptance coating $(T_s - T_c)$ and the substrate $(U - T_s)$, respectively. Thus

$$\Delta T = \Delta T_c + \Delta T_s . \tag{7}$$

Referring to figure 4 and making the same approximations which were made in order to derive eqs. (4) and (5), one obtains

$$(k_c/z_c)\Delta T_c = h_c(U - \Delta T - T_0) - E \quad , \tag{8}$$

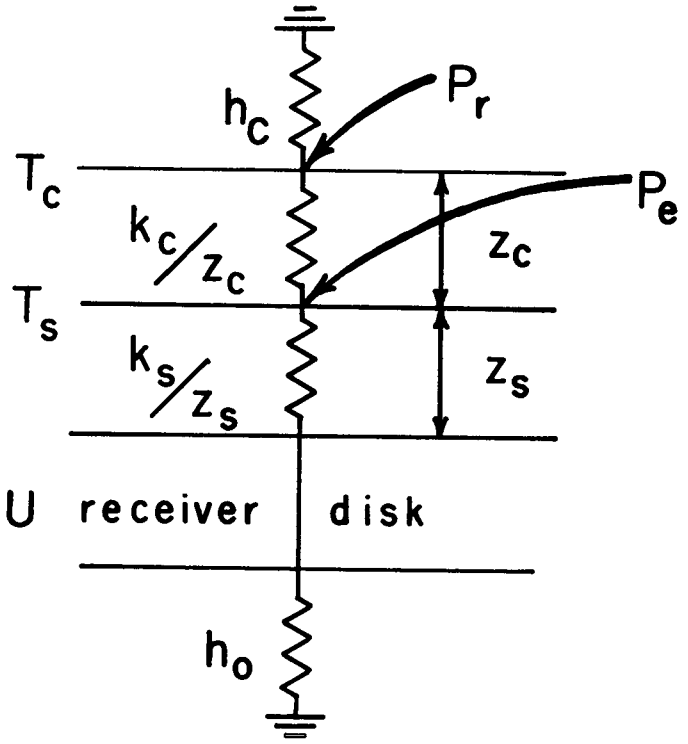

Figure 4. Network for analyzing one dimensional heat transfer through the substrate and high absorptance coating during radiant or electrical heating. T_c and T_s are the temperatures at the top of the high absorptance coating and electrically insulating substrate, respectively. U is the average temperature of the receiver at the point (ρ, ϕ). The arrow labled P_r represents the radiant power incident on the high absorptance coating and the arrow labled P_e represents the electrical power generated in the heater located between the coating and the substrate. In the analysis, E is used to represent the power density from either P_e or P_r.

and

$$(k_s/z_s)\Delta T_s = h_c(U - \Delta T - T_0) - E \ , \tag{9}$$

where z_s/k_s and z_c/k_c are the thermal resistances per unit reciprocal area of the substrate and the high absorptance coating, respectively. Now let

$$z/k = z_s/k_s + z_c/k_c \tag{10}$$

be the thermal resistance per unit reciprocal area of the substrate-coating combination. Equations (8) and (9) can be combined to yield

$$\Delta T(1 + zh_c/k) = z/k \left[h_c(U - T_0) - E\right] . \tag{11}$$

Substituting the expression for ΔT from eq. (11) into eq. (5), and letting

$$\gamma = (1 + zh_c/k)^{-1} \ , \tag{12}$$

yields

$$k_d \frac{\partial T}{\partial z}\bigg|_{z_d} = -\gamma\, h_c(U - T_0) + \gamma\, E. \tag{13}$$

Finally, substituting eqs. (4) and (13) into eq. (3) and letting

$$g^2 = (\gamma h_c + h_0) \ / \ z_d\, k_d \tag{14}$$

one obtains the approximate differential equation for the case of radiant heating,

$$\frac{1}{\rho}\frac{\partial}{\partial \rho}\left(\rho \frac{\partial U}{\partial \rho}\right) + \frac{1}{\rho^2}\frac{\partial^2 U}{\partial \phi^2} = g^2\ (U - T_0) - \gamma\ E/z_d\, k_d \ . \tag{15}$$

The case of electrical heating: referring to figure 4 and making the same assumptions mentioned in the discussion of the case of radiant heating, one obtains

$$(k_c/z_c)\Delta T_c = h_c(U - \Delta T - T_0) \tag{8a}$$

and

$$(k_s/z_s)\Delta T_s = h_c(U - \Delta T - T_0) - E \ . \tag{9a}$$

These can be combined to yield

$$\Delta T = \gamma \left[(z/k)h_c(U - T_0) - (z_s/k_s)\ E\right] \ . \tag{11a}$$

Substituting this result into eq. (5) yields

$$k_d \frac{\partial T}{\partial z}\bigg|_{z_d} = -\gamma\, h_c(U - T_0) + \gamma\ (1 + h_c z_c/k_c)\ E \ . \tag{13a}$$

Repeating the remaining steps as in the discussion of the case of radiant heating, one obtains

$$\frac{1}{\rho}\frac{\partial}{\partial \rho}\left(\rho \frac{\partial U}{\partial \rho}\right) + \frac{1}{\rho^2}\frac{\partial^2 U}{\partial \phi^2} = g^2\ (U - T_0) - \gamma(1 + h_c z_c/k_c)\ \ E/z_d\, k_d \ , \tag{15a}$$

as the approximate differential equation for the case of electrical heating.

Next make the substitution,

$$V = U - T_0 \tag{16}$$

in both eqs. (15) and (15a), to obtain equations of the form,

$$\frac{1}{\rho}\frac{\partial}{\partial\rho}\left(\rho\frac{\partial V}{\partial\rho}\right) + \frac{1}{\rho^2}\frac{\partial^2 V}{\partial\phi^2} - g^2 V = -Q(\rho, \phi) \tag{17}$$

for $0 \leq \rho \leq \rho_1$ and $0 \leq \phi \leq 2\pi$, where

$$Q(\rho, \phi) = \gamma \ell E(\rho, \phi) \,/\, z_d\, k_d \tag{18}$$

$$\text{where } \ell = 1 \tag{19}$$

in the case of radiant heating, and

$$\ell = \left(1 + h_c\, z_c/k_c\right) \tag{20}$$

in the case of electrical heating. It can be verified that the Green's function [14] for eq. (17) is

$$G(\rho, \phi; \rho_0, \phi_0) = \sum_{m=-\infty}^{\infty} \sum_{n=-\infty}^{\infty} A_{mn}\, I_m(g\rho)\, I_n(g\rho_0)\, e^{i(m\phi + n\phi_0)} - \frac{1}{2\pi} K_0\left\{g\left[\rho^2 + \rho_0^2 - 2\rho\rho_0 \cos(\phi-\phi_0)\right]^{\frac{1}{2}}\right\} \tag{21}$$

where the A_{mn} are determined by the boundary conditions and where I_n and K_n are the modified Bessel functions of order n. Physically, the Green's function describes the response at the point (ρ, ϕ) due to a unit point source at (ρ_o, ϕ_o). A useful property of the Green's function is that

$$V(\rho, \phi) = -\int_{\rho_0=0}^{\rho_1} \int_{\phi_0=0}^{2\pi} Q(\rho_0, \phi_0)\, G(\rho, \phi; \rho_0, \phi_0)\, \rho_0\, d\rho_0\, d\phi_0 \tag{22}$$

For a receiver with a radial thermopile, the boundary condition for the Green's function is

$$k_d \frac{\partial}{\partial\rho} G(\rho,\phi;\rho_0,\phi_0)\Big|_{\rho_1} = -h_1(\phi)\, G(\rho_1,\phi;\rho_0,\phi_0)\ , \tag{23}$$

where $h_1(\phi)$ is the heat transfer coefficient of the edge of the disk as a function of location. It is the sum of contributions from conduction down the thermopile legs, convection, and radiation. For simplicity and because of the high thermal conductivity of the receiver disk assume that $h_1(\phi)$ is independent of ϕ. Under this assumption it is convenient to define an averaged Green's function as

$$\bar{G}(\rho_1, \rho_0, \phi_0) = \int_{\phi=0}^{2\pi} G(\rho_1, \phi; \rho_0, \phi_0)\, d\phi\ . \tag{24}$$

Substituting eq. (21) into eq. (24) and carrying out the indicated integrations [15] yields

$$\bar{G}(\rho_1, \rho_0, \phi_0) = \sum_{n=-\infty}^{\infty} 2\pi\, A_{0n}\, I_0(g\rho_1)\, I_n(g\rho_0)\, e^{in\phi_0} - K_0(g\rho_1)\, I_0(g\rho_0)\ , \tag{25}$$

where the A_{0n} are still to be determined by the boundary condition [eq. (23)] which reduces to

$$k_d \frac{\partial \bar{G}(\rho_1, \rho_0, \phi_0)}{\partial \rho_1} = -h_1 \bar{G}(\rho_1, \rho_0, \phi_0) \ . \tag{26}$$

This requires that $A_{0n} = 0$ for $n \neq 0$, and

$$2\pi A_{00} = \frac{\left[\xi K_0 (g\rho_1) - K_1 (g\rho_1)\right]}{\left[\xi I_0 (g\rho_1) + I_1 (g\rho_1)\right]} \ , \tag{27}$$

where

$$\xi = h_1/gk_d \ . \tag{28}$$

Combining the above results and making use of the Wronskian relations among Bessell functions [16], results in

$$\bar{G}(\rho_1, \rho_0, \phi_0) = \frac{-I_0 (g\rho_0)}{g\rho_1 \left(\xi I_0 (g\rho_1) + I_1 (g\rho_1)\right)} \tag{29}$$

The voltage across the radial thermopile is given by

$$v = \int_{\phi = 0}^{2\pi} W(\phi) V(\rho_1, \phi) \, d\phi \ , \tag{30}$$

where $W(\phi)$ is the sensitivity (per unit angle) of the thermopile as a function of position around the edge of the receiver. Now, assuming that $W(\phi)$ is independent of ϕ, and combining eqs. (22), (24), (29), and (30) yields

$$v = \frac{2\pi W}{g\rho_1 \left(\xi I_0 (g\rho_1) + I_1 (g\rho_1)\right)} \int_{\rho_0 = 0}^{\rho_1} I_0 (g\rho_0) Q(\rho_0) \rho_0 d\rho_0 \ , \tag{31}$$

where

$$Q(\rho_0) = \frac{1}{2\pi} \int_{\phi_0 = 0}^{2\pi} Q(\rho_0, \phi_0) \, d\rho_0 \tag{32}$$

Now we will use this result to calculate the ratio of the thermopile voltages obtained when a quantity of radiant power is absorbed by the receiver and when the same quantity of electric power is absorbed. Let the radiant power density and electrical power density distributions be given by

$$E_r (\rho_0, \phi_0) = P_0 f_r (\rho_0, \phi_0) \ , \tag{33}$$

and

$$E_e (\rho_0, \phi_0) = P_0 f_e (\rho_0, \phi_0) \ , \tag{34}$$

respectively, where f_r and f_e have the dimensions of reciprocal area and P_0 is a quantity of power. Both f_r and f_e are defined to satisfy the relation,

$$\int_{\phi_0 = 0}^{2\pi} \int_{\rho_0 = 0}^{\rho_1} f(\rho_0, \phi_0)\, \rho_0\, d\rho_0\, d\phi_0 = 1 . \tag{35}$$

Combining eqs. (33) and (34) with eqs. (18),(31),(32), and letting v_r and v_e denote the thermopile voltages for the cases of radiant and electrical heating respectively, results in the expression,

$$v_r/v_e = \frac{\int_{\rho_0 = 0}^{\rho_1} I_0(g\rho_0) \int_{\phi_0 = 0}^{2\pi} f_r(\rho_0, \phi_0)\, d\phi_0\, \rho_0\, d\rho_0}{(1+h_c z_c/k_c) \int_{\rho_0 = 0}^{\rho_1} I_0(g\rho_0) \int_{\phi_0 = 0}^{2\pi} f_e(\rho_0, \phi_0)\, d\phi_0\, \rho_0\, d\rho_0} \tag{36}$$

First notice that the error arising from the fact that the radiant power and electrical power are each absorbed in different parts of the receiver depends only upon two parameters of the radiometer, g and $h_c z_c/k_c$. Furthermore, eq. (36) can be interpreted to mean that this source of error can be factored into two separate effects. The first of these will be called the relative responsivity effect, since it is described by $I_0(g\rho_0)$. The second effect is the increase in the emission of radiation during radiant heating over that during electrical heating due to the different temperature distributions that exist in the high absorptance coating during these two modes of heating. This will be called the excess emittance effect. It is described by $(1 + z_c h_c/k_c)^{-1}$.

The above results suggest that it may be worth-while to measure the excess emittance and relative responsivity errors in separate experiments. Indeed this is the case. Moreover, it turns out to be highly desirable to measure the excess emittance error and the error caused by the non-zero reflectance of the high absorptance coating in the same experiment, since it is very difficult to distinguish between the powers reflected from and emitted by the coating. Both of these power loss mechanisms affect the error in the same way. These points will be discussed in more detail when the experiment to measure the absorptance of the receiver is described.

Now we turn our attention to the theory of the measurement of the relative responsivity of the receiver. Ideally this will be measured by observing the variations in thermopile output as a point power source is applied at different locations on the receiver surface. Thus to describe a point source power input let

$$E(\rho_0, \phi_0) = P_0\, \delta(\vec{\rho} - \vec{\rho}_0) = \frac{P_0\, \delta(\rho - \rho_0)\, \delta(\phi - \phi_0)}{\rho_0} \tag{37}$$

where P_0 is a quantity of power, and δ is the Dirac delta distribution function. Combining eq. (37) with eqs. (18), (31), and (32) results in an expression for the responsivity as a function of position on the receiver,

$$\frac{v}{P_0} = \frac{W \gamma \ell\, I_0(g\rho)}{g\rho_1\, z_d\, k_d \left(\xi\, I_0(g\rho_1) + I_1(g\rho_1)\right)} \tag{38}$$

According to this equation, the variation in responsivity of the receiver is governed by the variations of the modified Bessel function, $I_0(g\rho)$. The variations of this function are small only when $g\rho \ll 1$: a condition satisfied by a good (useful) radiometer. We can, therefore, substitute the series expansions of I_0 and I_1 into eq. (38) and drop terms of order $(g\rho)^3$ and higher. The responsivity is then given by

$$F(\rho) = \frac{W \gamma \ell\, (1 + g^2 \rho^2/4)}{\rho_1\, z_d\, h_1\, (1 + g^2 \rho_1^2/4) + \frac{1}{2} \rho_1^2\, (\gamma h_c + h_0)} \tag{39}$$

In order to discuss the physical interpretation of this equation we will rewrite it in the form,

$$F(\rho) = 2\pi W \hat{R}(\rho) / (H_1 + H_c + H_0) \tag{40}$$

where

$$\hat{R}(\rho) = 1 + g^2 \rho^2/4 , \tag{41}$$

$$H_1 = 2\pi\rho_1 z_d h_1 \hat{R}(\rho_1) / \gamma\ell \tag{42}$$

$$H_c = \pi \rho_1^2 h_c/\ell , \tag{43}$$

$$H_0 = \pi\rho_1^2 h_0/\gamma\ell . \tag{44}$$

Recall that W is the thermopile sensitivity at the edge of the disk and notice that $\hat{R}(\rho)$ describes the relative responsivity of different locations on the surface of the receiver if the entire receiver is geometrically perfect and if its thermal parameters are independent of location. H_1, H_c, and H_0 can be interpreted as the thermal conductances from the edge, top and bottom surfaces of the receiver disk to its thermal environment, respectively. For instance, consider H_1. Here $2\pi\rho_1 z_d$ is the area of the edge of the disk, h_1 is the heat transfer coefficient from the edge of the disk, to the thermal environment of the disk, and $\hat{R}(\rho_1)/\gamma\ell$ is a correction factor.

It was assumed in the derivation of eq. (38) that the receiver is geometrically perfect and that its thermal parameters are independent of position, but in actual fact these parameters will vary with location in some unknown manner due to imperfections in materials and fabrication techniques. It is to be expected that z_s, z_c, and the thermal resistances of the joints where the thermopile junctions are attached to the receiver and its thermal environment will be subject to the largest variations. The differential change in γ,ℓ, and g due to differential changes in z_s and z_c are given by

$$d\gamma = -h_c\gamma^2 (dz_s/k_s + dz_c/k_c) \tag{45}$$

$$d(g^2) = h_c \, d\gamma/z_d k_d \tag{46}$$

$$d\ell = 0 \tag{47}$$

in the case of radiant heating, and

$$d\ell = h_c \, dz_c/k_c \tag{48}$$

in the case of electrical heating.

Notice that each of these is proportional to h_c. This fact will be significant later when we discuss cavity type receivers. Right now, however, we will pursue the analysis assuming that all of the geometric and thermal parameters of the receiver are independent of location on the receiver. Results obtained from this analysis will provide significant physical insight, and the amount by which the predictions of the analysis differ from experimental results is a measure of the variation of these parameters.

Equation (40) could have been written down without solving the differential equation of heat conduction; however, the exact form of eqs. (41), (42), (43), and (44) can only be obtained from the solution to the differential equation for a specific receiver geometry.

Now it is of interest to examine the order of magnitude of the various parameters in eq. (40). This will be done for the receiver configuration used to test the responsivity

to electrical heating. This receiver, shown in figure 5, is very similar to a receiver configuration described by Gillham [8] and later by Blevin and Brown [9]. Here z_d = 0.1 cm,

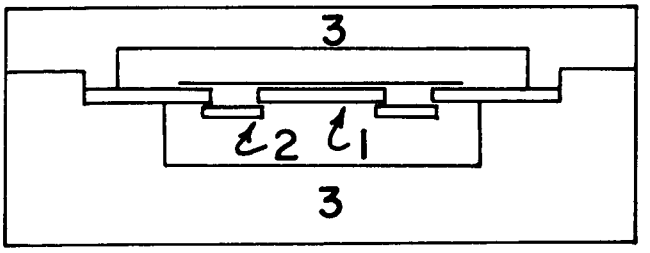

Figure 5. The receiver configuration used to examine the magnitude of the various parameters in eq. (40). 1 - receiver disk, 2 - radial thermopile, 3 - thermal environment of receiver.

ρ = 0.5 cm, and the top and bottom surfaces of the receiver are 0.3 cm and 0.5 cm from the thermal environment of the receiver, respectively. H_1, H_0, and H_c each have contributions from thermal radiation, air conduction and air convection. H_1 also has a contribution from conduction across thermopile legs, and heater leads. If the top and bottom surfaces of the receiver, as well as the thermal environment of the receiver are nearly black to infrared radiation,

$$h_c \simeq h_0 \simeq 4 \sigma T^3, \tag{49}$$

where T is the absolute temperature of some point on the receiver, and σ is the Stefan - Boltzmann constant. Thus (assuming that γ and ℓ are not much different from one) the thermal radiation contribution to h_c and h_0 is on the order of 0.6 mw/cm°C, so that the thermal radiation contribution to H_c and H_0 is on the order of 0.5 mw/°C. Empirical formulae which describe the contribution of air conduction and convection to H_c and H_0 do exist, but to apply them to this small geometry would be equivalent to extrapolating various experimental data parameters over many orders of magnitude. It is better instead to measure the responsivity of this receiver in air and in vacuum to determine the magnitude of the contribution of air conduction and convection to H_1, H_c, and H_0.

In order to analyze this experiment, we will rewrite eq. (40) to distinguish not between the thermal conductances of the top, bottom and edge of the receiver but between the modes of heat transfer which exist in vacuum and those which require air to exist. Let H_V denote the thermal conductance between the receiver and its environment in vacuum, and let H_A denote the thermal conductance between the receiver and its environment due to air conduction and convection. Thus

$$F_V = 2\pi W \hat{R}/H_V \tag{50}$$

and

$$F_A = 2\pi W \hat{R}/(H_V + H_A) , \tag{51}$$

where F_V and F_A are the responsivities to power applied at some point on the receiver in vacuum and air respectively, and where $\hat{R}$ is the relative responsivity at that point. Eliminating H_V between these equations yields,

$$H_A = 2\pi W \hat{R} \left(\frac{1}{F_A} - \frac{1}{F_V} \right) . \tag{52}$$

The receiver on which the measurements were made had a 20 junction copper-constantan (~40μv/°C) electroplated, radial thermopile, so $2\pi W \simeq 800$ μv/°C. F_A was measured to 0.0195 v/w and F_V was measured to be 0.0247 v/w, so $H_A \simeq 8$ mw/°C and air conduction and convection contributes approximately 10 mw/cm^2 °C to $\gamma h_c + h_0$.

Adding the contributions from radiation to that of air conduction and convection we obtain a value of approximately 11 mw/cm^2 °C for $\gamma h_c + h_0$. From this result and the fact that the receiver disk was aluminum ($k_d \simeq 2$ w/cm °C) we calculate that $g^2 \simeq 0.056/cm^2$ for this configuration. Thus if all of the geometric and thermal parameters of the receiver are independent of location on the receiver, the percentage difference between the responsivities at the edge and center of the receiver should be $g^2 \rho_1^2/4 \simeq 0.35\%$.

Now we will discuss some experimental data on the uniformity of responsivity of absolute radiometer receivers in light of the above analysis. Gillham [8] and Blevin and Brown [9] have described absolute radiometers with a receiver configuration similar to that which we have analyzed in detail. There are, however, three important differences in design. The first is that their aluminum receiver disks are only one half as thick as the receiver disk which we analyzed. Reference to eq. (14) shows that this difference would be expected to double g^2 and hence to double the maximum percentage difference in responsivity. The second difference is that the distance between the thermal environment and the top and bottom surfaces of their receivers are more than double those in the receiver which we investigated. Since air conduction makes by far the largest contribution to h_c and h_0, this difference should reduce g^2 by a factor of two. Thus the first two differences approximately cancel. The third difference is that Gillham and Blevin and Brown employed a thermopile whose 28 junctions were distributed approximately uniformly over the bottom surface of the receiver instead of a 20 junction radial thermopile. This difference should cause a significant decrease in the maximum difference in responsivity of 0.35% which we calculated, yet Gillham and Blevin and Brown report measuring a maximum variation in responsivity of 1%.

The above mentioned discrepancy between the predicted and measured maximum difference in uniformity in the radiometers of Gillham and Blevin and Brown, is probably due to the fact that some of the assumptions we made in deriving eq. (38) do not apply for their radiometers. As mentioned earlier, it is likely that the thermal resistances of the high absorptance coating, the substrate, and the joints where the thermocouple junctions are attached to the receiver and its thermal environment all vary with position over the receiver, due to variations in the thickness of the adhesive joints and coatings. The relative importance of these various components in increasing the non-uniformity of responsivity of the receiver cannot be estimated from the limited data which has been disclosed by the various authors.

In order to perform better than ± 0.5% accuracy irradiance measurements with a radiometer whose receiver is non-uniform in responsivity to 1%, it is necessary that the electrical and radiant power distributions be almost identical over the surface of the receiver. This requirement severely limits the types of radiant source and viewing geometries which the radiometer can accommodate. This in turn makes intercomparisons of different irradiance scales and radiant power scales difficult, if not impossible, since most of these scales are realized with considerably different source and viewing geometries. For instance, the laser power scales require that the receiver aperture not be irradiated at all.

As an example of the importance of having a highly uniform responsivity over the receiver, consider the measurement of the Stefan - Boltzmann constant reported by Blevin and Brown [7]. Of the twelve sources of error which they considered, the four largest uncertainties arose from the uncertainty in the thermodynamic temperature scale, the uncertainty in the calibration of the thermocouple, the uncertainty in the effect of diffraction, and the uncertainty in the effect of the non-uniformity of responsivity of the receiver, contributing uncertainties to the final result of 0.06%, 0.06%, 0.06%, and 0.05%, respectively. The first three of these corrections are source related, that is, they are uncertainties associated with the irradiance produced by the source at some point in space, and not with the way that the radiometer measures irradiance. Thus the largest radiometer related uncertainty in the measurement of the Stefan-Boltzmann constant was caused by the non-uniformity of responsivity of the receiver, even though the radiant and electrical power distributions were made as similar as possible under the constraints imposed by the radiometer design. This is seen to be even more significant when one realizes that the source related uncertainties do not contribute at all to other irradiance measurements, such as comparing two lamps or calibrating other detectors.

Finally, let us consider the uniformity of responsivity of a cavity type receiver. The receiver we have been discussing can be made into a cavity type receiver by affixing a top

to it as shown in figure 6. A top whose thermal properties are similar to those of the disk will be approximately isothermal, so as a first approximation h_c will be reduced by the configuration factor from the disk to the cavity opening which is typically on the order of 0.1. This means that g^2, and hence the contribution to the non-uniformity in responsivity described by $\hat{R}(\rho)$, can be reduced by almost a factor of two by incorporating the receiver

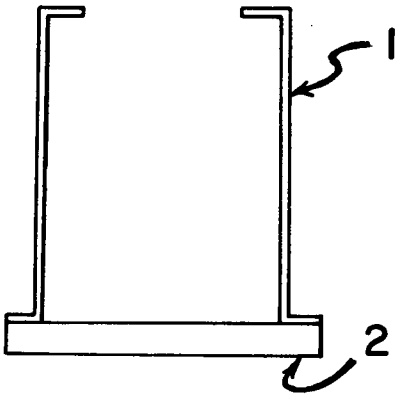

Figure 6. Cavity receiver made from the type of receiver that was analyzed theoretically in section 4.1. The upper cavity, 1, can be formed by drawing silver sheet, and it can be affixed to the receiver disk, 2, with a high thermal conductivity adhesive.

into a cavity configuration. However, we have shown that all of the contributions to the non-uniformity of responsivity of the receiver which arise from variations in z_s and z_d are proportional to h_c. Thus these contributions to the non-uniformity of responsivity of the receiver can be reduced by a factor equal to the configuration factor (0.1). It is harder to determine the effect of decreasing h_c on the contribution to the non-uniformity of the receiver due to variations in the thermal resistances of the joints where the thermopile junctions are attached to the receiver and its thermal environment. However as a first approximation, for a radial thermopile the decrease in non-uniformity would be proportional to the decrease in $\gamma h_c + h_0$, while for a thermopile whose junctions were distributed approximately uniformly over the bottom surface of the receiver, the decrease in non-uniformity would be proportional to the decrease in $\gamma h_c + h_1$.

From the discussion presented here, it should be clear that one of the more important design criteria for an absolute radiometer is a highly uniform receiver. A considerable amount of effort in the current program has been directed toward solving this problem.

Now let us turn our attention to the theory of the measurement of the corrections for the various sources of error affecting the detector. Let v_r be the thermopile voltage that is measured during radiant heating, then from conservation of energy the equation describing v_r can be written as,

$$v_r = S_r (P_r - \zeta_r P_r - \delta_r P_r) + S'_r P'_r \tag{53}$$

Here S_r is the average responsivity of the receiver to the quantity of radiant power, P_r, that enters the detector aperture and is incident on the receiver, and S'_r is the average responsivity of the receiver to the radiant power, P'_r, that does not enter the aperture but is incident on the detector case. The fraction of P_r that leaves the front surface of the receiver as radiant power is ζ_r and the fraction of P_r lost through all other mechanisms except conduction down the thermopile or radiation from the front surface of the receiver is δ_r.

A similar equation can be written for the thermopile voltage, v_e, measured during a period of electrical heating:

$$v_e = S_e (P_e - \zeta_e P_e - \delta_e P_e) + S'_e P'_e \ . \tag{54}$$

All of the terms in this equation are the electrical heating and loss equivalents of the radiant heating and loss terms in eq. (53) except for S'_e, which is the average responsivity of the receiver to the electrical power, P'_e, that is generated in the heater leads during electrical heating.

If v_r and v_e are made equal during the measurement, then

$$P_r = P_e S_e (1 - \zeta_e - \delta_e)/S_r (1 - \zeta_r - \delta_r) + (S'_e P'_e - S'_r P'_r)/S_r (1 - \zeta_r - \delta_r) \tag{55}$$

which can be expanded in a binomial series to yield

$$\begin{aligned} P_r &= P_e + P_e(\zeta_r - \zeta_e) + P_e(\delta_r - \delta_e) \\ &+ P_e(S_e - S_r)/S_r + S'_e P'_e/S_r - S'_r P'_r/S_r + \cdots \end{aligned} \tag{56}$$

The second term on the right-hand side of eq. (56) is the correction for the non-zero reflectance and non-zero thermal resistance of the coating of the receiver. The third term on the right-hand side of eq. (56) is the correction for other non-equivalent heat transfer mechanisms from the top surface of the receiver to its thermal environment, i.e., air conduction and convection. The fourth term is the correction for the variations in responsivity over the surface of the receiver that was discussed previously. The fifth term is the correction for lead heating during periods of electrical heating of the receiver, and the sixth term is the correction for the heating of the detector case by the radiation that does not enter the aperture during radiant heating. The higher order terms which have been omitted are interaction terms which in the case of well designed cavity receivers are smaller than 10^{-4}, and the modifications of the theory necessary to take them into account are trivial.

By dividing eq. (53) by eq. (54), setting $P_r = P_e$ and assuming that $S'_r P'_r$ and $S'_e P'_e$ are negligible, we obtain an expression for v_r/v_e which by comparison with eq. (36) (and under the same simplifying assumptions that were made in deriving eq. (36*) yields

$$(1 - \zeta_e - \delta_e)/(1 - \zeta_r - \delta_r) = (1 + h_c z_c/k_c) \ . \tag{57}$$

where h_c, z_c and k_c have been defined previously. Recall that h_c includes contributions both from air conduction and from radiation.

Equation (57) provides an estimate of the magnitude of the excess emittance error due to the different temperature distributions existing in the high absorptance coating during the periods of radiant and electrical heating. Such an estimate is useful when evaluating proposed detector designs. Experimental techniques for determining corrections with reliable uncertainties for both the radiation and the air conduction contributions to the excess emittance error are described in sections 4.3 and 4.4.

*This includes an implicit assumption that the high absorptance coating has zero reflectance.

4.2 Techniques for Measuring the Variation in Responsivity Over the Surface of the Receiver Disk.

In this section we will discuss two measurements which can be performed to determine the responsivity as a function of position over the surface of the receiver disk. Ideally, this measurement would be performed by introducing a fixed quantity of power into different portions of the receiver, and recording the thermopile output voltage for each of the positions. An approximation to this idealization which is readily realized is to irradiate the high absorptance coating of the receiver with the image of an aperture which itself is irradiated by the image of the filament of a lamp, as shown in figure 7. However, there are some problems with this technique. The first problem is that we are not measuring just the variations in responsivity of the receiver disk, but instead we are measuring some combination of the desired quantity and the variations in reflectance and thermal resistance of the high absorptance coating. The second problem is that it is very difficult to irradiate much of the interior of the cavity, and even more difficult to know exactly what location on the interior surface is actually being irradiated. The third problem concerns the quality of the image with which the receiver is irradiated. It is possible that the area around the image will not be of negligible irradiance compared to the image itself, due to scattering and/or aberrations in the imaging optics. Thus in order to obtain reliable results by this technique it is necessary to map out the irradiance as a function of position in the image plane, and if the irradiance in the area around the image is not negligible, to apply corrections for it.

The consequences of measuring the responsivity as a function of position by this technique without knowing the irradiance distribution in the image plane can be more serious in the case of the detector we have developed, than in the case of the detectors of Gillham [8], Blevin and Brown [9, 17], and Bischoff [10].† Since the detector developed on this project has a radial thermopile, it has a higher responsivity at the edge than at the center of the receiver disk. Thus if the irradiance around the image decreases with increasing distance from the image at just the right rate, the decreased power incident on the receiver when the image falls near the edge of the receiver would just compensate for the increased responsivity of the edge of the receiver and the output voltage of the detector would be independent of the location on the receiver upon which the image falls. This would result in an underestimate of the maximum variation in responsivity over the receiver, and more seriously, an underestimate of the uncertainty in irradiance measurements due to this source of error. However, the detectors of Gillham, Blevin and Brown, and Bischoff have receivers whose responsivities decrease near the edge of the receiver. Consequently, the two effects described above would add in this case, and the maximum variation in responsivity over the receiver would be overestimated. Since all of these authors use this measured maximum variation in responsivity to calculate an uncertainty due to this source of error, they obtain, at worst, an overly conservative limit of error. However, if they were to apply corrections based upon the receiver responsivity distribution measurements in the absence of image plane irradiance distribution measurements, it is clear that they would underestimate the limit of error associated with this source of error.

There is a second technique, which while not ideal, does have some advantages. It is to put two heaters at different locations on the receiver disk (under the high absorptance coating), and to compare the thermopile outputs with the same quantity of power being dissipated in one heater or in the other. Modern materials advances make this technique more practical than in the past. Now the heater and leads need not be wire coils and/or evaporated metal films. Instead, silver or graphite filled enamels can be used. These have the advantage that they can be quickly applied like paints, and that they can be quickly removed with solvents. The silver filled materials yield resistances on the order of 10^{-2} ohms per square, which are handy for heater leads. The graphite filled materials can yield resistances greater than 10^{4} ohms per square which are ideal for small area heaters. This technique shows promise in reducing the first and third problem mentioned above.

†Strictly speaking these comments apply only to non-cavity receivers.

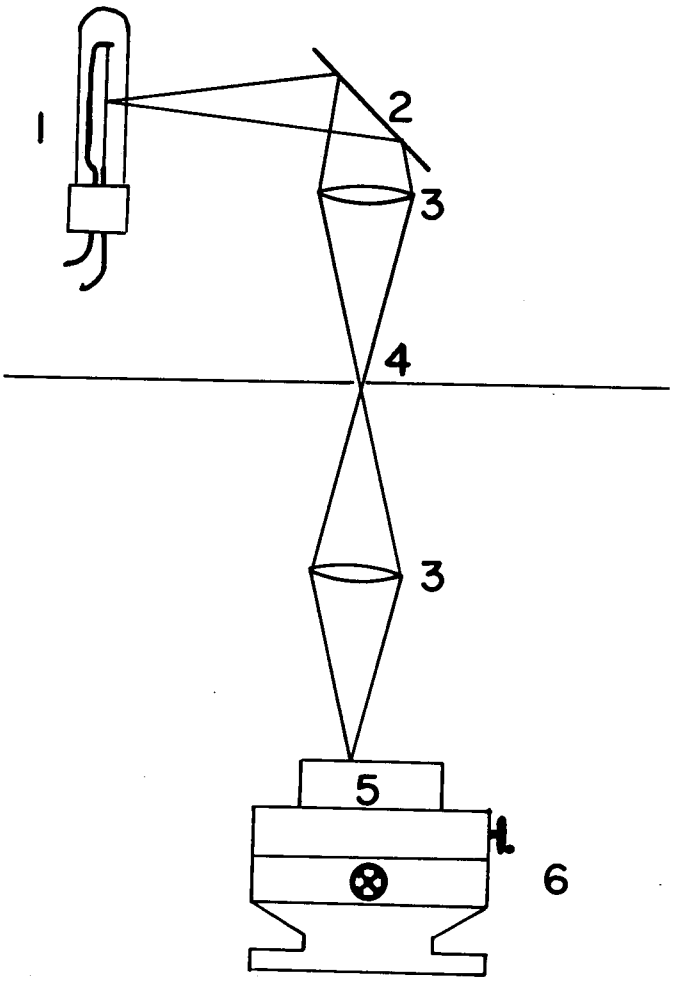

Figure 7. Apparatus for measuring the responsivity over the surface of the receiver disk. 1 - tungsten strip filament lamp, 2 - plane mirror, 3 - lenses, 4 - aperture in opaque screen, 5 - radiometer, 6 - indexing table.

4.3 Techniques for Measuring the Non-Equivalent Heat Losses from the Receiver due to the Emission and Reflection of Electromagnetic Radiation

In this section we will describe a very versatile technique which is a combination and extension of two previously described techniques [18, 19], and which can be used to determine a single correction for the cumulative effect of two different sources of error. The first source of error is the imperfect absorption of radiant flux by the receiver due to the non-zero reflectance of the high absorptance material with which it is coated. The second source of error is the emission of more flux when the receiver is heated radiantly than when it is heated electrically due to the non-zero thermal resistance of the high absorptance material with which it is coated. The theory of these sources of error has been investigated in section 4.1.

The second term on the right hand side of eq. (56), $P_e(\zeta_r - \zeta_e)$, is the correction for the cumulative effect of these two sources of error. Figure 8 is a diagram of the type of apparatus which can be used to determine ζ_r and ζ_e. The flux from a tungsten strip lamp is focused on an aperture. The flux passing through the aperture is in turn focused through the hole in the hemispherical mirror onto the receiver of an electrically calibrated detector. The hemispherical mirror can be rotated to reflect the flux which leaves the front surface of the receiver either back onto the receiver or onto a portion of the thermal environment of the receiver which has been coated with a high absorptance material. A shutter located in the plane of the aperture is synchronized with a switch in the electrical heater circuit so that the receiver is heated radiantly when the shutter is open and electrically when it is closed.

The spherical aberation of the hemispherical mirror place some restrictions on the type of receivers that can be accomodated by this type of apparatus. The receiver must be large enough to intercept all of the flux that has passed through the hole in the hemispherical mirror, and been reflected back toward the receiver. Blevin has mentioned this point. In the case of a cavity type receiver, reflected flux can leave the receiver from any point in the plane of the cavity opening. Thus the image of the aperture must be smaller than the cavity opening, and the cavity opening must be surrounded by a flat annular region that is coated with a high absorptance material.

The apparatus has four distinct states. If the shutter is open and the hemispherical mirror is so oriented that the flux leaving the front surface of the receiver is reflected onto the thermal environment of the receiver, the thermopile output is given by

$$A_r = S_r P_r (1 - \zeta_r - \delta_r) + \varepsilon_r' \tag{58}$$

where ε_r' is an offset voltage (note that the case heating effect is not present). Now if the mirror is rotated so that the flux leaving the front surface of the receiver is reflected back onto the receiver, the thermopile output is

$$B_r = S_r P_r (1 - \zeta_r - \delta_r) + S_r \zeta_r P_r (1 - \zeta_r - \delta_r) + \varepsilon_r' \ . \tag{59}$$

assuming spherical mirror reflectance is unity. When the shutter is closed (electric heater on) and the hemispherical mirror is so oriented that the flux leaving the front surface of the receiver is reflected onto the thermal environment of the receiver, the thermopile output is given by

$$A_e = S_e P_e (1 - \zeta_e - \delta_e) + \varepsilon_e \ , \tag{60}$$

where the offset voltage ε_e includes the voltage generated by the power dissipated in the heater leads ($S_e' P_e'$ in section 4.1).

When the mirror is rotated so that the flux leaving the front surface of the receiver is reflected back onto the receiver, the thermopile output is

$$B_e = S_e P_e (1 - \zeta_e - \delta_e) + S_e \zeta_e P_e (1 - \zeta_r - \delta_r) + \varepsilon_e \ . \tag{61}$$

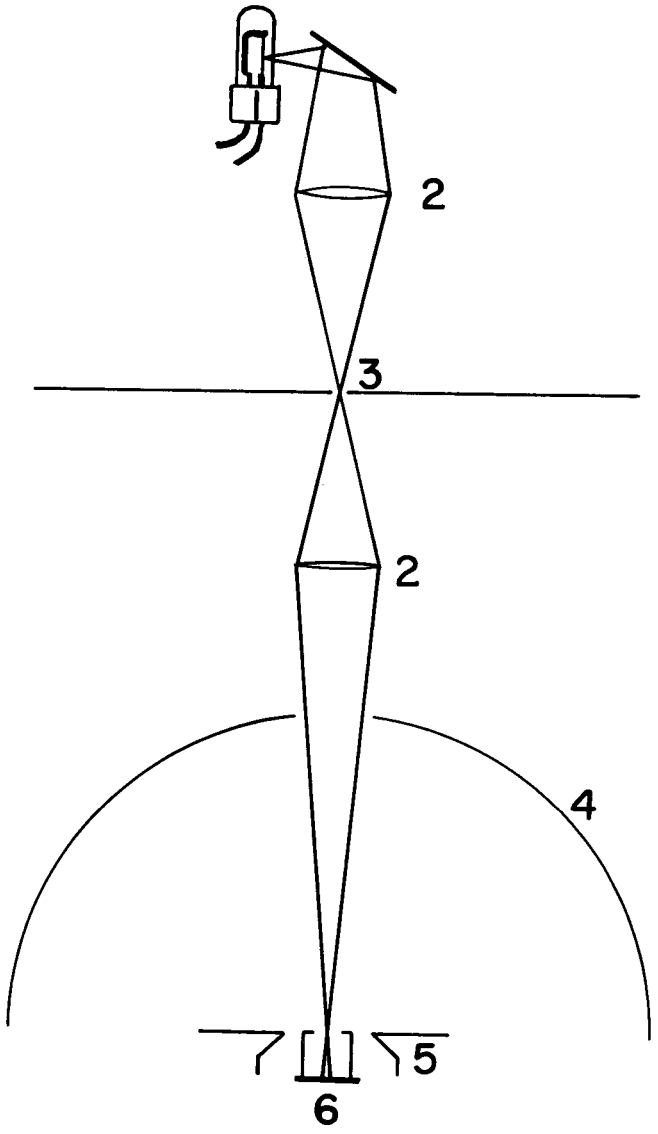

Figure 8. Apparatus for measuring the reflectance plus the excess emittance of the receiver. 1 - tungsten strip filament lamp, 2 - lenses, 3 - aperture in opaque screen, 4 - hemispherical mirror, 5 - thermal environment of receiver, 6 - cavity receiver. Notice that to avoid chromatic aberations, the lens between the screen and the hemispherical mirror should be replaced by a reflectance focusing element.

Thus

$$\zeta_r = (B_r - A_r)/(A_r - \varepsilon_r') \tag{62}$$

and

$$\zeta_e/(1 - \zeta_e - \delta_e) = (B_e - A_e)/(A_e - \varepsilon_e)(1 - \zeta_r - \delta_r) \ . \tag{63}$$

Once δ_r and δ_e are known, ζ_e can be obtained. We discuss techniques for measuring δ_r and δ_e in the next section.

4.4 Techniques for Measuring the Non-Equivalent Heat Loss from the Receiver due to Air Conduction and Convection

In this section we will describe a technique which can be used to determine a correction for the non-equivalent heat loss from the receiver due to air conduction and convection. The third term on the right-hand side of eq. (56), $P_e(\delta_r - \delta_e)$, is the correction for this source of error. Figure 9 is a diagram of the type of apparatus which can be used to determine δ_r and δ_e. The flux from a tungsten strip lamp is focused on an aperture. The flux passing through the aperture is in turn focused through the window in an evacuable chamber onto the receiver of an electrically calibrated radiometer. It is essential for this measurement that the lamp be stable in radiance over fairly extended periods of time, whereas, this was not a requirement for the measurement described in the preceding section. Furthermore, it is necessary that the receiver have the same thermal environment during this measurement as it had during the measurement described in the preceding section. If this is the case, then when the chamber is at ambient pressure, the thermopile output voltage during radiant heating will be given by

$$C_r = S_r P_r(1 - \zeta_r - \delta_r) + \varepsilon_r \ , \tag{64}$$

where the offset voltage ε_r includes the case heating effect. The thermopile output voltage during electrical heating will be given by

$$C_e = S_e P_e(1 - \zeta_e - \delta_e) + \varepsilon_e \ . \tag{65}$$

However, when the chamber is evacuated, the thermopile output voltage during radiant heating will be given by

$$D_r = S_r P_r(1 - \zeta_r) + \varepsilon_r \ , \tag{66}$$

and the thermopile output voltage during electrical heating will be given by

$$D_e = S_e P_e(1 - \zeta_e) + \varepsilon_e \ . \tag{67}$$

Thus

$$\delta_r = (1 - \zeta_r)(D_r - C_r)/(D_r - \varepsilon_r) \ , \tag{68}$$

and

$$\delta_e/(1 - \zeta_e - \delta_e) = (D_e - C_e)/(C_e - \varepsilon_e) \ . \tag{69}$$

Notice that ζ_r was already expressed in terms of measurable quantities in eq. (62) so δ_r can be calculated. However, in order to express δ_e in terms of measurable quantities, it is necessary to solve eqs. (63) and (69) simultaneously. The result is

$$\zeta_e = E/(1 + E + F) \ , \tag{70}$$

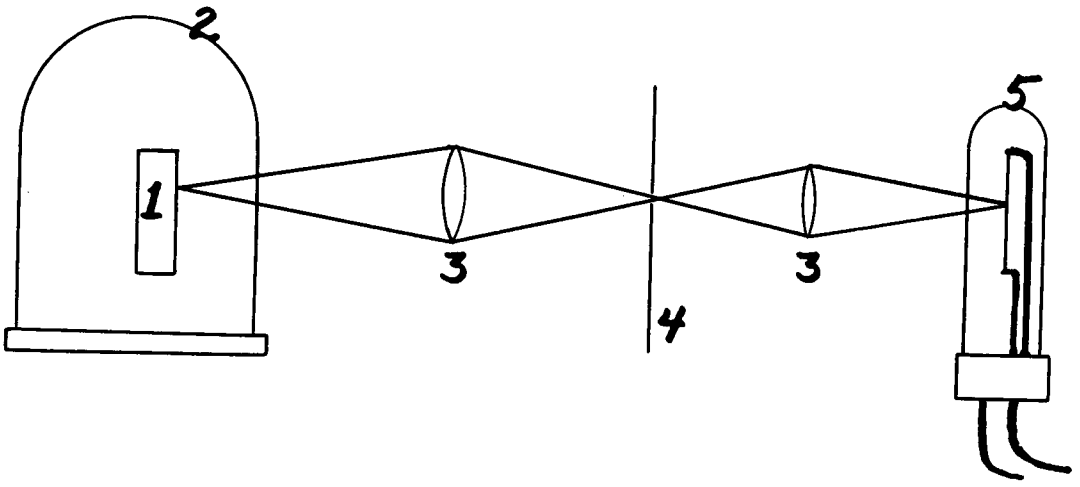

Figure 9. Apparatus for measuring the non-equivalent heat loss from the receiver due to air conduction and convection. 1 - detector 2 - evacuable bell jar, 3 - lenses, 4 - aperture in opaque screen, 5 - tungsten strip filament lamp.

and

$$\delta_e = F/(1 + E + F) , \tag{71}$$

where

$$F = (D_e - C_e)/(C_e - \varepsilon_e) , \tag{72}$$

and

$$E = (B_e - A_e)/(A_e - \varepsilon_e)(1 - \zeta_r - \delta_r) . \tag{73}$$

4.5 Techniques for Measuring Corrections for the Remaining Sources of Error

The two remaining sources of error that will be considered in this section are the power dissipated in the heater leads, and the radiant flux incident on the thermal environment of the receiver. Both of these sources of error are basically different from the sources of error discussed in sections 4.2, 4.3, and 4.4. Those sources of error can be characterized as imperfect absorption and sensing by the receiver of the power that it is supposed to sense; whereas, the two sources of error discussed here can be characterized as a sensing by the receiver of power that it is not supposed to sense.

Gillham [20] has devised the lead configuration shown in figure 10, in order to measure the lead heating correction. During a period of electrical heating the circuitry external to the heater leads is arranged so that equal currents, of magnitude 1/2, flow into the heater through leads 1 and 3, and out of the heater through leads 4 and 6, while the voltage across the heater is measured between leads 2 and 5. Letting S'_e be the responsivity of the receiver to the power, P'_e, generated in the heater leads, the voltage across the thermopile during this period is given by

$$G_e = S_e P_e(1 - \zeta_e - \delta_e) + S'_e P'_e . \tag{74}$$

To measure the lead heating correction, the external circuitry is rearranged so that a current of magnitude 1/2 flows from lead 1 to lead 3, and from lead 4 to lead 6, while maintaining zero voltage between leads 2 and 5. Then the detector is irradiated so that the voltage across the thermopile,

$$G' = S_r P_r(1 - \zeta_r - \delta_r) + S'_e P'_e \tag{75}$$

is just equal to G_e. Then the external circuit is open so that the current ceases to flow in leads 1, 3, 4, and 6. Now the thermopile output voltage is given by

$$G_r = S_r P_r(1 - \zeta_r - \delta_r) . \tag{76}$$

Thus the voltage error during the period of electrical heating is $G'_r - G_r$. The reason for irradiating the detector during this measurement is to eliminate any error arising from nonlinearity in S'_e.

In order to measure the error caused by the radiant flux incident on the thermal environment of the receiver, Gillham [21] built a heater onto the front of his radiometer. A problem with this technique is that it is difficult to get the power distributions under radiant and electrical heating to be the same in the vicinity of the aperture. An alternate approach is to build a "dummy" aperture holder identical to the aperture holder in every way except that it has no aperture. Then the receiver can be alternately shuttered from and exposed to the radiation from the lamp. However since there is no aperture, none of the radiation from the lamp can be incident on the receiver. Thus any change in thermopile voltage is

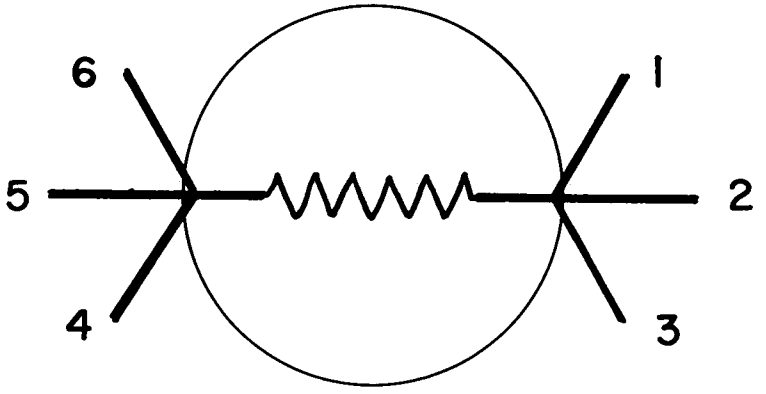

Figure 10. Heater lead configuration for measuring the effect of lead heating. 1, 3, 4, and 6 - current leads, 2 and 5 - voltage leads, 7 - heater.

due to heating of the thermal environment of the receiver including the aperture holder. This experiment is the exact compliment of the technique described for measuring the lead heating error. If H is used to represent the thermopile voltage output during these measurements, and if P_r' and S_r' represent the power supplied to the thermal environment of the receiver, and the responsivity of the receiver to that power respectively, then all of the equations describing this measurement can be obtained from eqs. (74), (75), and (76) by substituting H for G, r for e, and e for r at every occurrence.

5. Electrically Calibrated Radiometer #10 and the Third International Pyrheliometer Comparisons

In this section we will describe Electrically Calibrated Radiometer (ECR) #10. The design of this radiometer differs in some important respects from the final design which evolved during this project, and the radiometer is no longer functioning. However, since it did participate in the Third International Pyrheliometer Comparisons at Davos, Switzerland in September of 1970 (IPC 1970) [22], its construction, design, and testing, as well as the results obtained during IPC 1970 are of more than passing interest.

For the most part ECR #10 was built and tested in accordance with the principles described in the preceding sections of this report. Construction of the radiometer is described in section 5.1, measurements of correctors for the various systematic errors affecting the radiometer are described in section 5.2, and the measurements performed during IPC 1970 are described in section 5.3.

5.1 Construction of the Radiometer

Figure 11 is a cross sectional view of ECR #10. The water cooled heat shield was constructed from two pieces of copper plate and soldered together. A cross section through the solder joint is shown in figure 12. A top view of the main chassis is shown in figure 13. The aperture insert shown in figure 14, was eloxed from hardened steel, and the edge of the aperture itself was ground. The resulting hole was traced on a Talyrond [23] and found to be circular to within ±20 μ inches. The average diameter of the hole was measured to be 0.10296" with a ±0.00003" limit of error. Referring back to figure 11, the aperture

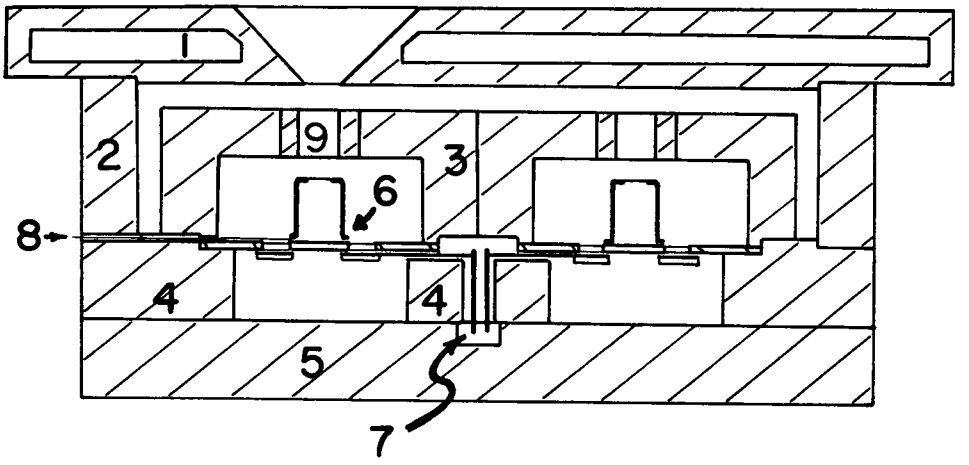

Figure 11. Cross section of ECR #10 (Full Scale). 1 - water-cooled heat shield, 2 - heat shield support, 3 - aperture insert holder, 4 - main chassis, 5 - back plate, 6 - receiver assembly, 7 - thermopile leads, 8 - heater leads, 9 - aperture insert.

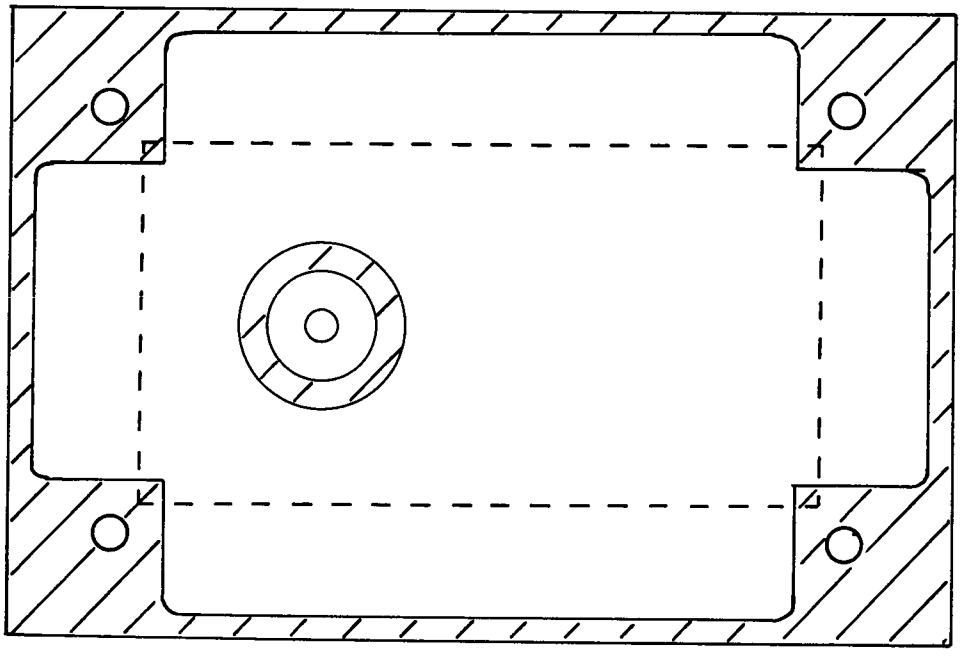

Figure 12. Cross section through solder joint of water-cooled heat shield (Full Scale).

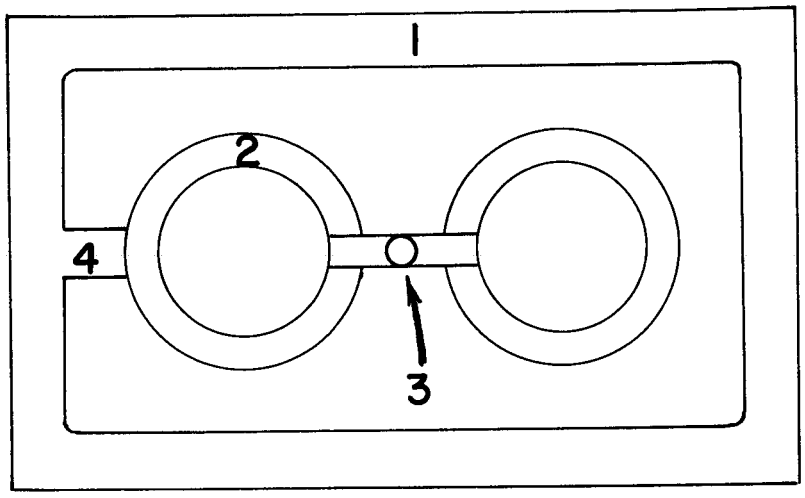

Figure 13. Top view of main chassis. 1 - recess for heat shield support, 2 - recess for receiver assembly, 3 - access for thermopile leads, 4 - access for heater leads (Full Scale).

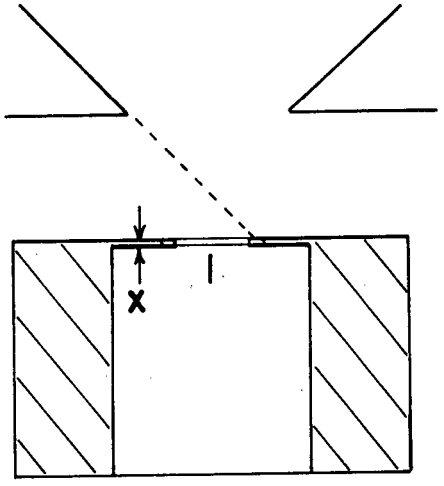

Figure 14. Magnified view of the aperture insert. 1 - aperture, x - 0.006 inches. The dotted line shows the relation of the aperture to the water-cooled heat shield.

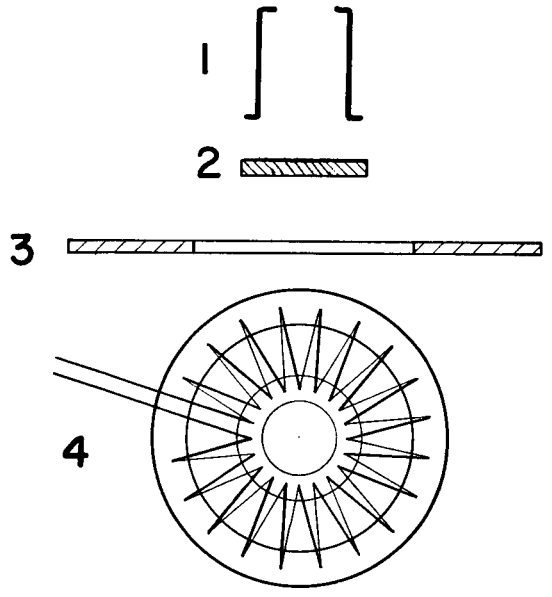

Figure 15. Exploded view of the receiver assembly. 1 - upper cavity, 2 - receiver disk, 3 - thermopile cold junction support, 4 - thermopile (rotated through 90° for better view).

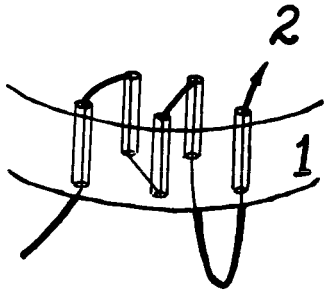

Figure 16. Isometric view of edge of thermopile jig - 1, showing wire - 2 being sewn through holes in jig.

insert holder (3) and the receiver assembly (6) are attached to the main chassis (4) with silver filled silicon rubber adhesive in order to assure good thermal contact, while still permitting the parts to be disassembled if necessary.

Figure 15 is an exploded view of the receiver assembly, which consists of the receiver disk, the cold junction support, the radial thermopile, and the upper cavity. The radial thermopile was made by electrodepositing copper on constantan wire. The theory of such thermopiles is well known [24], but considerable difficulty was encountered in attaching these thermopiles to the receiver disk and the cold junction support, both of which were made of anodized aluminum. The general plan of construction was as follows.

A 5 mil diameter constantan wire was sewn through holes drilled in a 1 mm thick jig as shown in figure 16 (materials from which jig was made will be discussed below). One side of the jig was then coated with a suitable lacquer to prevent any copper from being plated on the wire which was on that side of the jig. The jig was then placed in a solution of copper sulfate and sulfuric acid in water, and the wire on the uncoated side of the jig was electroplated. After plating was complete, an adhesive was applied to the thermopile in the region where it would contact the receiver disk, and the thermopile-jig combination was clamped to the disk until the adhesive had hardened. Then the jig was removed by melting or dissolving it in a suitable solvent.

One of the problems encountered was that the bond between the adhesive and the disk was attacked by many of the solvents which were tried. Part of this problem was that the disk was made of anodized aluminum in order to allow good thermal contact between it and the pile without it shorting electrically. Many adhesives do not bond well to anodized aluminum. Another contributing factor was that the adhesive layer was quite thin and its edges were unprotected from the solvent.

A number of different adhesives were tried including epoxy, cellulose acetate dissolved in acetone, shellac dissolved in ethyl alcohol, and sodium silicate cement. Among the different jig material-solvent combinations that were tried were polystyrene-benzene, cellulose acetate-acetone and ethyl cellulose-ethyl alcohol. Attempts were made to construct the jig of materials which melt at low temperatures without swelling. Rosin and a number of waxes were tried alone and in combinations. The problem here was that the jig would either be too brittle for drilling or too soft to keep the wires from cutting through it.

Only two techniques which were considered suitable resulted from this work. In the first of these techniques calcium carbonate was suspended in a sodium silicate solution and used as an adhesive. The jig was made of polystyrene, and was dissolved away in benzene with no noticeable effect on the silicate adhesive. It is difficult to get this adhesive to wet the thermocouple leads, but it can be done. In the other technique, dental molding compound was cast in an aluminum ring. By itself the molding compound was too brittle to be useful, but held in compression by the ring it could be drilled with no fear of breakage. Epoxy was used as an adhesive. The molding compound was removed by immersion in molten beeswax. The temperature of the beeswax is important. Higher temperatures favor the disintegration and complete removal of the molding compound, but if the temperature is too high, the epoxy is softened sufficiently for the thermopile to loosen. The optimum temperature of the molten beeswax has not yet been determined.

In the end, neither of these techniques was considered ideal, and the general plan of construction was modified as follows. The constantan wire was sewn through a polystyrene jig to which was glued an outer ring and an inner disk of 5 mil cellulose acetate as shown in figure 17A. The polystyrene jig was then dissolved in benzene leaving the thermopile held loosely in shape by the cellulose acetate ring and disk. To these a small quantity of epoxy adhesive was applied and the pile was clamped to the receiver disk as shown in figure 17B. This method of clamping resulted in the desired intimate contact between the receiver disk and the thermopile. The disadvantage of this technique is that the cellulose acetate disk increases the thermal mass of the sensitive area of the detector. However, the ease of construction and the increased strength of the bond justifies its use.

The configuration of the heater and heater leads on the receiver is shown in figure 18. The leads between the thermopile cold junction support and receiver disk were 3 mil diameter platinum wire arranged in the Gillham configuration. They are brought over the surface of the receiver to the heater by a commercially available silver filled lacquer of high elec-

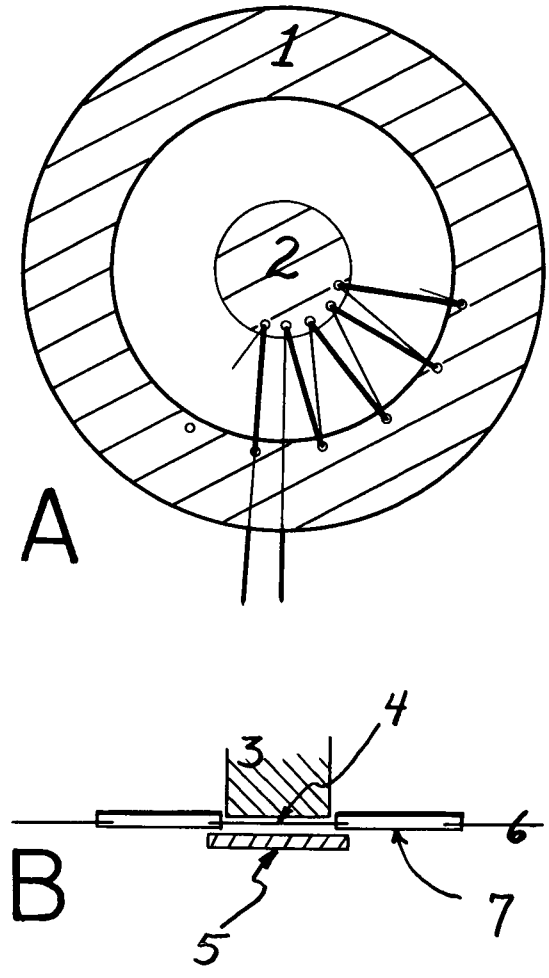

Figure 17. A - Thermopile supported by cellulose acetate ring - 1, and disk - 2. B - Method of clamping the thermopile to the receiver disk while the epoxy hardens. 3 - teflon rod, 4 - cellulose acetate disk, 5 - receiver disk, 6 - cellulose acetate ring, 7 - thermopile.

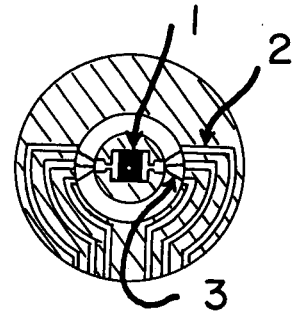

Figure 18. The configuration of the heater and the heater leads on the receiver disk and the thermopile cold junction support. The thermopile is not shown. 1 - heater, 2 - silver filled lacquer heater lead, 3 - three mil diameter platinum wire.

trical conductivity which was applied by spraying though a mask. The heater itself was made by suspending graphite in a lacquer vehicle and was also applied by spraying through a mask.

The upper cavity was drawn from 10 mil thick silver and finished by eloxing. It and the receiver disk were coated with Eppley-Parsons Optical Black Lacquer [23] and were joined by a silver filled epoxy adhesive chosen to yield the lowest thermal resistance between the receiver disk and the upper cavity.

In order to use ECR #10 as a pyrheliometer, it was necessary to construct the special view limiting aperture shown in figure 19. Also constructed was a special support plate

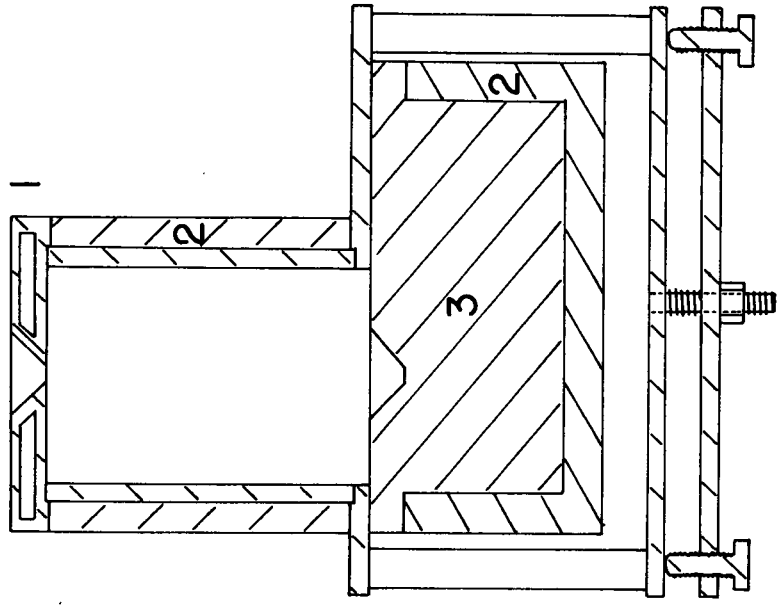

Figure 19. Pyrheliometer view limiting aperture and mount for ECR #10. 1 - water-cooled heat shield, 2 - polyurethane foam insulation, 3 - ECR #10.

that allowed both ECR #10 and one of the PACRAD [11] detectors of J. M. Kendall, Sr. to be attached to it at the same time, and the whole assembly mounted on an equatorial mount which Kendall provided. A hole in the tube supporting the view limiting aperture was provided so that visual observation of the alignment of the detector relative to the solar axis could be made with a dentist's mirror. Since ECR #10 could be aligned independently of the equatorial mount, it was possible for both radiometers to be aligned with the solar axis.

5.2 Measurements of Corrections for the Various Errors Affecting ECR #10

In this section we will describe the measurements which were performed on ECR #10 to determine corrections for the various errors affecting it. Unfortunately, an unstable-resistance-short circuit developed across the heater in ECR #10 before the apparatus to measure the non-equivalent effect of air conduction and convection was completed, so this measurement could not be performed. The consequences of this circumstance will be discussed. All of the other types of measurements described earlier in this report were performed.

First we describe the measurement of the responsivity of the receiver disk as a function of position. This measurement was performed at the point in the construction of the radiometer just before the heater and the upper cavity were to be affixed to the receiver disk. To prepare the receiver disk for this measurement, it was spray coated with Eppley-Parsons Optical Black Lacquer following the instructions supplied by the manufacturer. This coating was removed after the measurement, so that the heater could be applied. After the heater was applied the receiver disk was recoated in the same manner.

The apparatus used in this measurement was of the type described in section 4.2. The image of the aperture on the receiver was nominally one mm in diameter. However, measurements of the irradiance as a function of position in the image plane showed a significant amount of scattered flux outside the area of the image, and a correction (to be described later) for this effect was necessary. The indexing table on which the detector was mounted was driven by a stepping motor. The detector-thermopile voltage was amplified with a linear dc nanovoltmeter, read with a digital voltmeter (DVM), and recorded on punched paper tape with a teletype.

The points on the receiver disk of ECR #10 at which measurements were made are shown in figure 20. (All distances in the figure are measured in thousandths of an inch.) First the detector was aligned on the indexing table so that the image of the aperture was centered at the point (0,y) on the receiver disk (relative to the coordinate system which has its origin at the center of the disk, see figure 20), and so that the indexing table motion was along the x axis, where y was set at either 0, ±0.050", or ±0.100". The data acquisition sequence was as follows:

1) move table x inches to right, wait 90 seconds, read DVM, punch paper tape,
2) move table x inches to left, wait 90 seconds, read DVM, punch paper tape,
3) move table x inches to left, wait 90 seconds, read DVM, punch paper tape,
4) move table x inches to right, wait 90 seconds, read DVM, punch paper tape,
5) repeat sequence starting at step 1.

Thus the data format on the paper tape was

$V_1,_1(-x,y)$
$V_1,(0,y)$
$V_1,_3(x,y)$
$V_1,_4(0,y)$
.
.
.

$V_{i,1}(-x,y)$
$V_{i,2}(0,y)$
$V_{i,3}(x,y)$
$V_{i,4}(0,y)$
.
.
.
$V_{n,4}(0,y)$

where $V_{i,j}(f(j)x,y)$ is the $j^{\underline{th}}$ measurement in the $i^{\underline{th}}$ series of measurement of the thermopile voltage for irradiation incident at the point $(f(j)x,y)$ on the surface of the receiver disk, and where n is one-fourth of the total number of measurements. The function f(j) has three values, 0, ±1, and is defined in the data sequence above. The values of x were chosen from 0.050", 0.080", 0.100" depending upon the value of y as can be seen from figure 20.

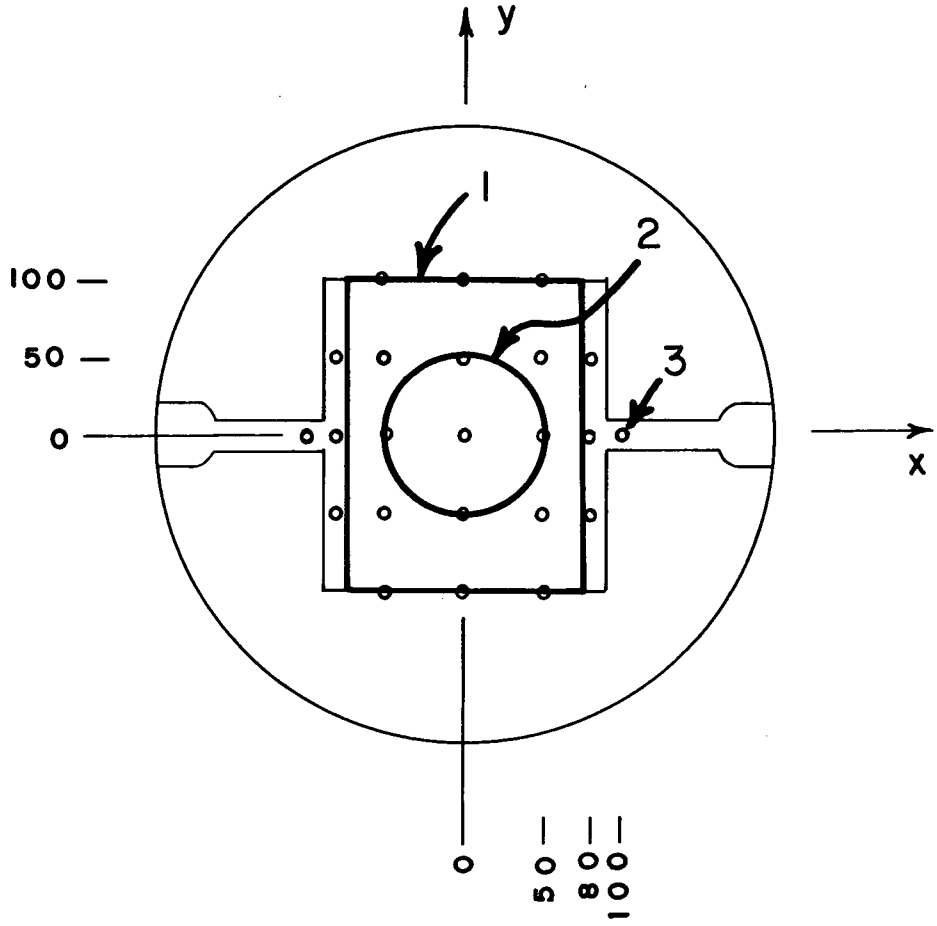

Figure 20. The points on the surface of the receiver of ECR #10 at which the relative responsivity of the receiver was measured - 3, the area that was heated by solar radiation at Davos - 2, and the area of the electric heater - 1. The scale is in thousandths of an inch and the origin is in the center of the receiver.

Next the detector was rotated 90° so that the table motion was along the y axis and so that the image of the aperture was centered on the point (0,0) of the receiver disk (relative to the coordinate system of figure 20). The data acquisition sequence described earlier was again employed resulting in the paper tape format,

$$
\begin{aligned}
&V_{n+1,1}(0,-y)\\
&\quad\vdots\\
&V_{i,1}(0,-y)\\
&V_{i,2}(0,0)\\
&V_{i,3}(0,y)\\
&V_{i,4}(0,0)\\
&\quad\vdots\\
&V_{m,4}(0,0)
\end{aligned}
$$

The values of y were either 0.050", or 0.100", and m-n is one-fourth of the total number of measurements performed with the table motion along the y axis.

From the data on the paper tape we calculated,

$$R(f(j)x,y;0,y) = \sum_{i=1}^{n}\left[\frac{2\,V_{i,j}(f(j)x,y)}{V_{i,2}(0,y) + V_{i,4}(0,y)}\right], \tag{77}$$

and

$$R(0,f(j)y;0,0) = \sum_{i=n+1}^{m}\left[\frac{2\,V_{i,j}(0,f(j)y)}{V_{i,2}(0,0) + V_{i,4}(0,0)}\right], \tag{78}$$

where $f(j) = j-2$, and $j = 1,3$.

During the above described measurements the radiometer did not have a window over its receiver in order to avoid any errors due to scattering by the window. Consequently, the radiometer was not well shielded from atmospheric micro-turbulence, and the data was subject to considerable noise from this source. Since long measurement periods of between eight to sixteen hours were required to obtain the desired signal to noise ratio in the calculated quantities, $R(x,y;0,y)$ and $R(0,y,0,0)$, the entire apparatus was automated. Now we discuss how these quantities were used to calculate the relative responsivity of the receiver.

Let P be the power within a 3 mm diameter circle concentric with the image, let $\bar{S}(x,y)$ be the relative responsivity of the receiver at the point (x,y), let $P'(x,y)$ be the power incident on the receiver outside of the 3 mm diameter circle concentric with the image, when the center of the image is at the point (x,y), and let $\bar{S}'(x,y)$ be the average relative responsivity of the receiver to $P'(x,y)$. Thus, using the techniques developed in section 4.1 to express the thermopile voltage in terms of responsivities,

$$R(x,y;0,y) \simeq \frac{P\bar{S}(x,y) + P'(x,y)\,\bar{S}'(x,y)}{P\bar{S}(0,y) + P'(0,y)\,\bar{S}'(0,y)}, \tag{79}$$

and

$$R(0,y;0,0) \simeq \frac{P\bar{S}(0,y) + P'(0,y)\,\bar{S}'(0,y)}{P\bar{S}(0,0) + P'(0,0)\,\bar{S}'(0,0)}. \tag{80}$$

where $\bar{S}(0,0)$ is arbitrarily chosen to be unity. Next multiply eq. (79) by eq. (80), expand the result in a binomial series and approximate $\bar{S}'(0,0)$ and $\bar{S}'(x,y)$ by $\bar{S}(x,y)$ to obtain

$$R(x,y;0,y)\,R(0,y;0,0) \simeq \bar{S}(x,y)\,[1 + (P'(x,y) - P'(0,0))/P]. \tag{81}$$

The approximations are justified because it will turn out that P'(0,0) and P'(x,y) are small compared to P, and that $\bar{S}(x,y)$ varies less than one percent over the surface of the receiver.

In order to determine the quantity, (P'(x,y)-P'(0,0))/P in eq. (81), which is a scattering correction, we must measure the irradiance as a function of position in the image plane. The apparatus was modified to do this. Two different detectors were employed. A vacuum thermopile detector with a CaF_2 window and a 0.2 x 2 mm receiver (stopped down to 0.2 x 1 mm) was used to map out a relative distribution of scattered flux, and a windowless thermopile detector with a 3 mm diameter receiver of fairly uniform sensitivity over its surface was used to determine the constant by which the relative distribution should be multiplied to obtain the distribution of scattered flux as a percent of the power contained in a 3 mm diameter circle surrounding the image. The nanovoltmeter in the apparatus was replaced by a lock-in amplifier, and a chopper was inserted into the radiation beam between the lamp and aperture when using the vacuum thermopile.

The points at which measurements were made with the different detectors are shown in figure 21. A number of different functions were fit to the vacuum thermopile data using a non-linear fitting routine, in an attempt to find a simple function, f(x,y), which represented the data fairly well.

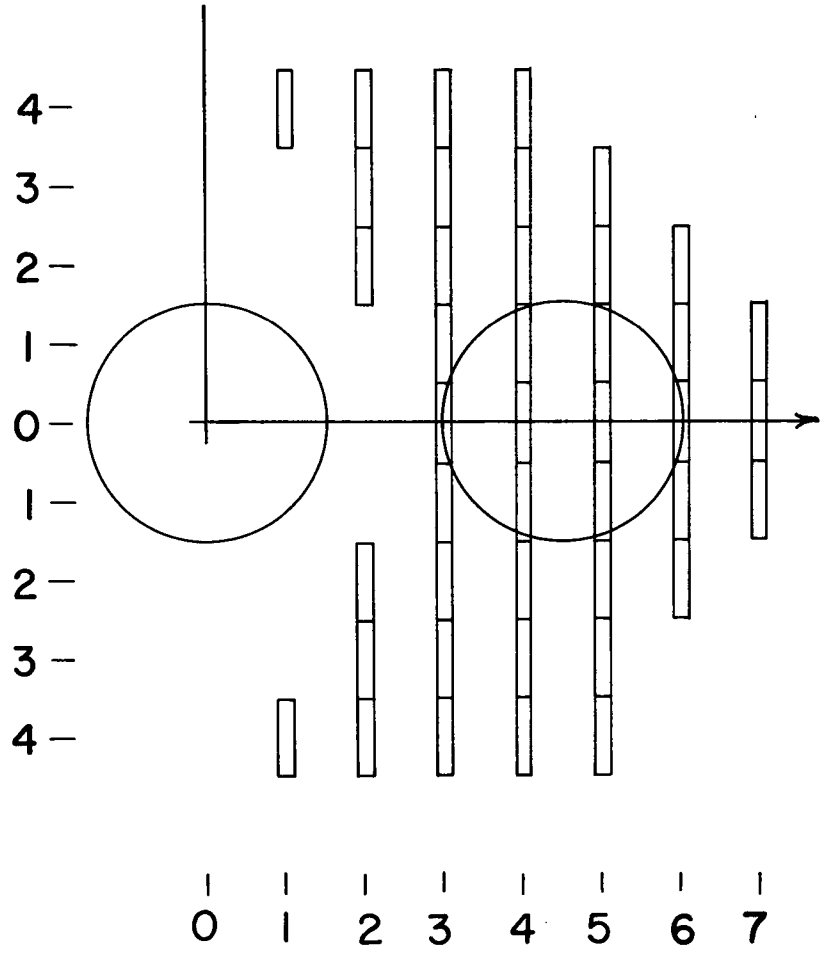

Figure 21. The points in the plane of the image of the aperture at which the flux scattered outside of the area of the image was measured. The scale is millimeters and the origin is the center of the image. The circles represent the positions of the large detector (3 mm diameter) and the rectangles represent the positions of the small detector (0.2 x 1 mm).

The function finally chosen was normalized in the following manner. Let

$$I(A) = \int\int_A f(x,y)\, dxdy, \tag{82}$$

where A is the surface in the (x,y) plane over which the integration is to be performed. For the normalization procedure, the surface A was a 3 mm diameter circle with its center displaced 4.5 mm from the center of the image of the aperture. It was required that I(A) be equal to the output voltage of the 3 mm diameter detector when displaced 4.5 mm from the center of the image, divided by the output voltage of the same detector when at the center of the image. In this way I(A) was made equal to the ratio of the power incident on surface A to that incident on a 3 mm diameter region concentric with the center of the image. Thus

$$P'(0,0) = P\ I\ (A_{00}), \tag{83}$$

and

$$P'(x,y) = P\ I\ (A_{xy}), \tag{84}$$

where A_{xy} is the surface in the plane of the image that is occupied by the receiver of the electrically claibrated radiometer when the center of the image is located at the point (x,y) of the receiver, minus the 3 mm diameter circular area surrounding the image, and A_{00} is similarly defined.

Substituting eqs. (83) and (84) into eq. (81), and using the first two terms of a binomial expansion results in an approximate expression for the relative responsivity,

$$\bar{S}(x,y) = R(x,y;0,y)\ R(0,y;0,0)\ (1 + I(A_{00}) - I(A_{xy})), \tag{85}$$

in terms of quantities based upon measurements. In evaluating $I(A_{xy}) - I(A_{00})$, it is not necessary to integrate over all of A_{xy} and A_{00}. All that is necessary is to integrate over the areas where A_{xy} and A_{00} do not overlap. Thus

$$I(A_{xy}) - I(A_{00}) = I(A_1) - I(A_2), \tag{86}$$

where A_1 and A_2 are defined in figure 22. This is the reason that measurements were performed only at the points shown in figure 21, when determining f(x,y). These were the only points for which the values of f(x,y) would affect the final result. (Spot checks that had been conducted previous to the measurement showed that f(x,y) was symmetric about the image to within ±10%).

Table 1: The values of the scattering correction for the points (x,y)* at which the responsivity as a function of position was measured.

y/x	-100	-80	-50	0	50	80	100
100			0.0014	0.0011	0.0014		
50		0.0010	0.0006	0.0003	0.0006	0.0010	
0	0.0011	0.0007	0.0003	0.0000	0.0003	0.0007	0.0011
-50		0.0010	0.0006	0.0003	0.0006	0.0010	
-100			0.0014	0.0011	0.0014		

*The distances x and y are measured in thousandths of an inch from the center of receiver.

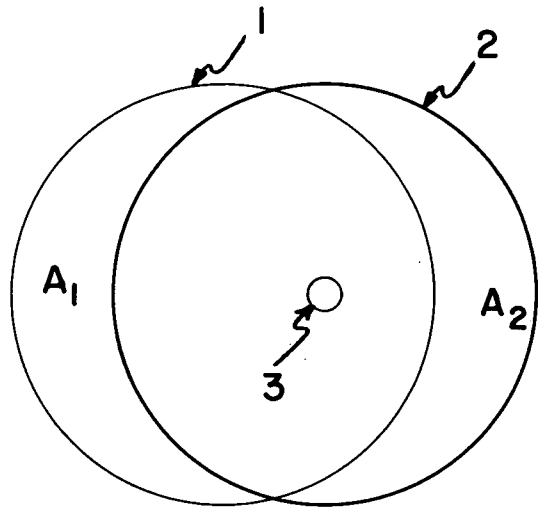

Figure 22. The definition of the areas, A_1 and A_2. 2 - the area of the receiver disk when concentric with 3 - the image of the aperture. 1 - the area of the receiver disk when displaced from area 2. A_1 and A_2 are the portions of 1 and 2 that do not intersect.

The values of the scattering correction, $I(A_{00}) - I(A_{xy})$, computed from eq. (86) are listed in table 1, for the points (x,y) shown in figure 20. The principal sources of error affecting these values are the residuals of the fit of f(x,y) (including the ±10% deviations from symmetry about the image of the aperture), and the three-sigma uncertainty in the normalization of I(A) due to the poor signal-to-noise ratio in the measurements made with the 3 mm diameter detector. This uncertainty was ±66% of I(A). The values of $\bar{S}(x,y)$ calculated according to eq. (85) are tabulated in table 2.

Table 2: The measured values of the relative responsivity, $\bar{S}(x,y)$ as a function of position* over the surface of the receiver of ECR #10.

y/x	-100	-80	-50	0	50	80	100
100			0.9969	0.9994	0.9986		
50		1.0006	0.9998	1.0000	0.9994	1.0004	
0	1.0010	1.0002	0.9981	1.0000	0.9998	1.0008	1.0021
-50		1.0022	0.9997	1.0005	1.0000	1.0016	
-100			1.0000	1.0003	0.9993		

*The distances x and y are measured in thousandths of an inch from the center of receiver.

The three-sigma uncertainties associated with the $R(\underline{x},y;0,y)$ and $R(0,y;0,0)$ data ranged about 0.03%. The estimated limit of error in the $\bar{S}(x,y)$ data is ±0.2% for the points on outer edge of the measured area, decreasing to zero at the center.

The areas on the receiver's surface that absorb the electrical power from the heater and the radiant power from the sun were shown in figure 21. The power density within these areas is quite uniform in both cases, so the average responsivity for the case of electrical heating was calculated as

$$\bar{S}_E = \left\{ \sum_{\substack{x\in\{-50,\ 0,\ 50\} \\ y\in\{-50,\ 0,\ 50\}}} \bar{S}(x,y) \quad + 0.5 \sum_{\substack{x\in\{-50,\ 0,\ 50\} \\ x\in\{-100,\ 100\}}} \bar{S}(x,y) \right\} \Big/ 12 \tag{87}$$

and the average responsivity for the case of solar heating was calculated as

$$\bar{S}_S = \left\{ \bar{S}(0,0) + 0.25\left[\bar{S}(-50,0) + \bar{S}(0,-50) + \bar{S}(0,50) + \bar{S}(50,0) \right] \right\} \Big/ 2 \tag{88}$$

where x and y are measured in thousandths of an inch. The values computed in this fashion are $\bar{S}_e = 0.9995$ and $\bar{S}_s = 0.9998$.

The correction for the variations in responsivity over the receiver of ECR #10 at Davos is just $\bar{S}_e/\bar{S}_s - 1 = -0.0003$ with an estimated limit of error of ±0.0010.

A measurement was also performed on ECR #10 to determine the responsivity of the cavity top relative to that of the center of its receiver disk. This was done after construction of the detector was completed, by covering the ring on the cavity top that surrounds the aperture with a ring of one thousandth inch thick transparent tape, and painting a heater onto this ring. The heater configuration is shown in figure 23. Nearly equal quantities

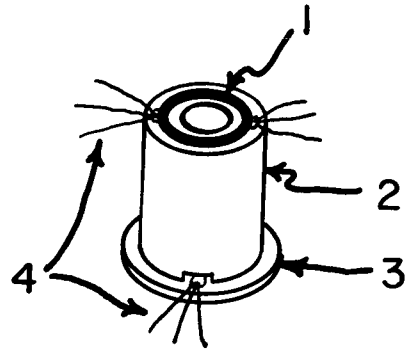

Figure 23. The configuration of the heater on the cavity top for the measurement of the responsivity of the cavity top relative to the center of receiver disk. 3 - the receiver disk, 2 - the cavity top, 1 - the heater on the cavity top, 4 - heater leads.

of power were alternately dissipated in each heater. These quantities of power were adjusted so that the steady state voltage across the thermopile was independent of which heater the power was dissipated in. The ratio of the responsivity of the cavity top to that of the center of the receiver disk was calculated as the reciprocal of the ratio of the power dissipated in the cavity top heater to that dissipated in the receiver disk heater. This ratio was 0.9699 with a three sigma uncertainty of ±0.0020.

In order to calculate an exact correction for this effect it is necessary to know the responsivity as a function of position over the cavity top, and the quantities of flux reflected from the coating of the receiver disk to different parts of the cavity top. However, we can calculate an approximate correction and a limit of error from the data that we do have. The relative responsivity of the cavity top that we have measured is a lower limit, due to the fact that it was measured at the point most remote from the thermocouple, and due to the fact that the thermal resistance of the tape reduced the measured value from the true value. Similarly we do not know the exact reflectance of the coating of Eppley-Parsons Optical Black Lacquer on the receiver disk, but we do know that it can range from less than two percent up to about five percent [24]. An upper limit for the correction for this effect is obtained by assuming that the reflectance of the coating is five percent, and that all of the reflected flux is detected with the lower limit of responsivity. In this case, the receiver would detect 95% + 5% of the flux as 95% + 4.85%, so the maximum correction factor for this effect would be 1.0015. We assumed a correction of 0.0008 with an estimated limit of error of ±0.0008.

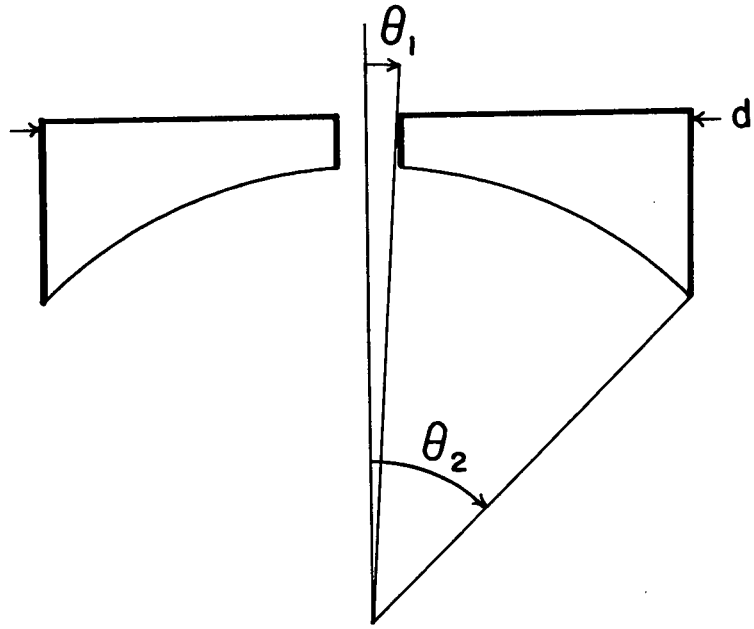

Figure 24. The spherical mirror used in the reflectance plus excess emittance apparatus. $\theta_1 = 2.8°$, $\theta_2 = 45.0°$, d = 7.0".

Now we will describe the measurements of the reflectance plus excess emittance correction for ECR #10. An apparatus similar to that described in section 4.3 was used. The dimensions of the spherical mirror (not a full hemisphere) are shown in figure 24. This type of mirror was used because it was felt that a full hemisphere would prevent adequate observation of the alignment of the receiver relative to the mirror. Ideally, separate measurements would also be made on the same apparatus using a mirror which formed the other half of the hemisphere. However, for the receiver of ECR #10, these measurements were not necessary. Since its interior was coated with Eppley-Parsons Optical Black Lacquer [23], which tends to be a retor-reflector for normally incident radiation [25], almost all of the reflected and excess emitted flux leaves the receiver after but one reflection. This flux is confined to a solid angle much smaller than that collected by the mirror. Of course a small correction has to be applied, as does a correction for the flux which passes through the hole in the mirror. Both of these corrections, the sum of which is equal to 0.10% with an estimated limit of error of ±0.10%, were based upon the data in reference 25.

The image of the aperture was nominally 2 mm in diameter. It is important that a negligible amount of flux fall outside an area 5 mm in diameter centered on the image. Any flux outside this region would be incident on the cavity top, and would cause the apparatus to measure a linear combination of the reflectance plus excess emittance of the cavity aperture and top instead of just that of the aperture. In order to measure a correction for this effect, a detector with a flat, ring shaped receiver of 5.0 mm ID and 10 mm OD was constructed. First the detector was aligned so that the image of the aperture was incident on the ring, and then the thermopile voltage with the shutter opened, v_1, and with the shutter colosed, v_0, was recorded. Next the detector was aligned so that the image passed through the hole in its center. Again the thermopile voltage with the shutter opened, v_1', and with it closed, v_0', was recorded. The detector had no window, and was not shielded from the air currents in the room for the same reasons mentioned in the description of the responsivity as a function of position measurements. So again signal to noise was a problem, and the apparatus was automated and let to run overnight.

The percentage of flux scattered out of the image into a ring with a 5.0 mm ID and 10.0 mm OD is given by $(v_1' - v_0')/(v_1 - v_0)$. This ratio was 0.1% with a three sigma uncertainty of 0.3%. Since the cavity top ring that surrounds the receiver aperture was coated with a specular black paint of about 3% reflectance, the correction for the scattered flux reflected by the cavity top is 0.00% with an estimated limit of error of ±0.01%.

Once the scattered flux correction was measured, ECR #10 was aligned in the apparatus and measurements were performed in accordance with the discussion in section 4.3. Since no measurements were made to determine δ_e and δ_r, it was assumed that $\delta_r = \delta_e + 0.1\% \pm 0.1\%$. In this case, eq. (71) can be approximated by

$$\zeta_e \simeq E' \, (1 - \zeta_r - 0.001)/(1 - E'), \tag{89}$$

where

$$E' = (B_e - A_e)/(A_e - \varepsilon_e) \, , \tag{90}$$

and where ζ_r is given by eq. (70).

Again it was necessary to run the apparatus overnight in order to achieve a satisfactory signal-to-noise ratio. Seven separate measurement runs were performed, yielding the seven mean values, 0.26%, 0.26%, 0.39%, 0.26%, 0.23%, 0.30%, and 0.26% for $\zeta_r - \zeta_e$. The standard deviations of these seven mean values ranged from 0.02% to 0.04%. A number of different statistical tests on this data show that it is very likely that a variable systematic error that has not been taken into account is present in the data [26]. Under these circumstances, the recommended estimate of the population mean is the simple average of the mean values of the seven runs. This average, 0.28%, is used as the correction for the reflectance plus excess emittance error. Since the calculated three-sigma interval (0.28% ± 0.06%), does not span the range of the seven mean values, we will use ± 0.11% as an estimated limit of error for the correction.

The receiver thermal environment heating and lead heating corrections were measured in accordance with the procedures described in section 4.5. The dummy aperture holder that was used is shown in figure 25. A high intensity total irradiance lamp [27] was used to irradiate the detector during the dummy aperture holder and lead heating measurements. Since the plane of the aperture was only 40 cm away from the lamp, almost twice as much irradiance was incident on the view limiting aperture as on the plane of the aperture, whereas for solar irradiance measurements the same irradiance is incident on both surfaces. To check for errors from this effect, the dummy aperture heating measurement was run with and without the view limiting aperture affixed to the detector. The result was the same in both cases, indicating that all of the effect arises in the aperture holder, probably in the thin ring surrounding the aperture. The correction for this effect is -0.33% with a three sigma uncertainty of ± 0.02%. The lead heating correction was measured to be 0.02% with a three sigma uncertainty of ± 0.04%.

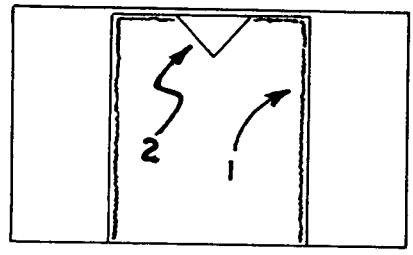

Figure 25. The dummy aperture holder. 1 - black coating on interior of dummy aperture holder (also on interior of aperture holder), 2 - 45° half-angle polished aluminum core to simulate the effect of the hole on emitted flux.

To summarize the corrections, we can rewrite eq. (56) as

$$P_r/P_e \simeq \left[1 + (\zeta_r - \zeta_e) + (\delta_r - \delta_e) + (S_e - S_r)/S_r + P'_e S'_e/S_r P_e - P'_r S'_r/P_e S_r\right] \tag{91}$$

The right side of eq. (91) is the correction factor by which the power measured during electrical heating must be multiplied to obtain the power incident on the receiver during radiant heating, once it has been adjusted so that the thermopile voltage is the same during both radiant and electrical heating.

Table 3 contains a summary of each of the corrections that contribute to the correction factor, and the estimated limits of error (three sigma limits in some cases) associated with them.

Table 3: A Summary of the Corrections for the Various Sources of Error for ECR #10.

Component of Error	Correction	Limit of Error
Uniformity of Responsivity		
$(S_e - S_r)/S_r$		
a) receiver disk	-0.0003	±0.0010
b) cavity top	+0.0008	±0.0008
Reflectance Plus Excess Emittance		
$(\zeta_e - \zeta_r)$		
a) collected by mirror	+0.0028	±0.0011
b) lost by mirror	+0.0010	±0.0010
Air Conduction Non-equivalence		
$(\delta_e - \delta_r)$	+0.0010*	±0.0010
Case Heating		
$-P_r'S_r'/P_eS_e$	-0.0033	±0.0002
Lead Heating		
$P_e'S_e'/P_rS_r$	+0.0002	±0.0004

*Estimated

In obtaining these corrections, P_e and P_r, and S_e and S_r have been interchanged in the last two terms of eq. (91). Since these corrections are small, this introduces negligible error. The value of the correction factor calculated according to eq. (9) from the values in table 3 is 1.0022 with an estimated limit of error of ± 0.0055.

5.3 The Participation of ECR #10 in the Third International Pyrheliometric Comparisons

In this section we describe the data obtained from ECR #10 during the Third International Pyrheiometer Comparisons at Davos, Switzerland.

Tables 4 and 5 contain data taken on September 11, 1970 as a check on the linearity of the radiometer. Kendall's electronics were used. The receiver of the radiometer was heated electrically with quantities of power corresponding to 113 mw/cm^2 and 78 mw/cm^2 irradiance, respectively. The calibration constant*, K, of the radiometer at these two levels of irradiance was 0.550 w/cm^2 mv ± 0.002 w/cm^2 mv. Notice that the quantity C_f = 18.682 cm^{-2},

*that is, the number of watts/cm^2 per millivolt of thermopile output.

which is used in calculating K, is the product of the reciprocal area of the detector aperture and the correction factor† for the detector.

Experiments were conducted on September 16, in order to calibrate the span of the strip chart recorder that was used to record the thermopile voltage in millivolts per chart division. A schematic diagram of the experiment is shown in figure 26. A computer program was written to perform a least squares fit of a quadratic equation to this data. The data itself, the coefficients of the linear and quadratic terms in the equation, and a comparison between the experimental values and the values computed from the quadratic equation are all contained in table 6.

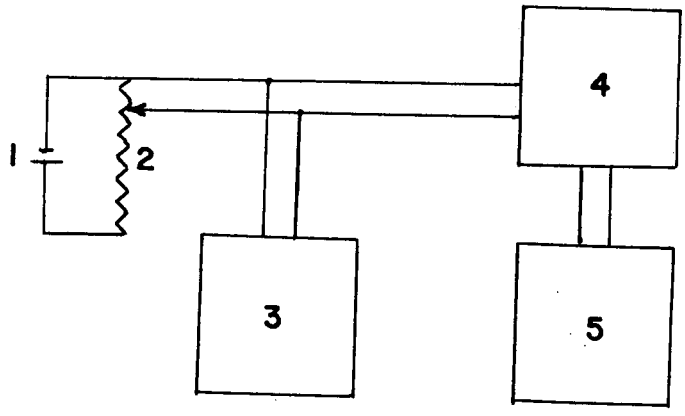

Figure 26. Schematic diagram of strip chart recorder linearity calibration. 1 - battery, 2 - variable resistor, 3 - Fluke Differential Voltmeter, 4 - Keithley Microvolt Ammeter, 5 - strip chart recorder.

The solar irradiance measurements were taken in the following manner: During the periods when the Ångstrom 210 pyrheliometer was taking data, the receiver of the NBS instrument was continuously heated by insolation. During the rest periods, the view limiting aperture was closed and the receiver was heated electrically for calibration purposes. Thus, a continuous strip chart recording of alternate periods of electrical and radiant heating was obtained; each period of radiant heating lasting about thirteen minutes. During the periods of electrical heating of the receiver, the voltage across the heater and the voltage across a 1000 ohm standard resistor in series with the heater were read on the Fluke Differential Voltmeter [23] and written in pen on the strip chart next to the trace. During the periods of radiant heating of the receiver, the time at which the strip chart pen crossed one of the time scale divisions on the strip chart was written on the chart next to that division, and the division was marked.

The data reduction technique is the following: The average value of the strip chart trace is calculated for each period of electrical heating and for the last twelve or twelve and one-half minutes of each period of radiant heating. For the periods of electrical heating, the equivalent irradiance of the electrical power is calculated as 18.682 cm^{-2} times the product of the voltages across the receiver heater and the standard resistor divided by 1000 ohms. This quantity is the value of irradiance which would result in the same strip chart recorder value during a period of insolation of the receiver as was recorded during the period of electrical heating of the receiver. For a period of insolation, the irradiance is calculated as the sum of the equivalent irradiance for an

†The correction factor that was applied at Davos was 1.0035. Later measurements yielded the value obtained in section 5.2.

adjacent period of electrical heating of the receiver and the value of the irradiance difference, ΔE, which corresponds to these adjacent periods of electrical and radiant heating. The irradiance difference was calculated from tables 4 and 5 as 0.55 mw/cm^2 mv times the difference in voltage which corresponds to the two different strip chart recorder values. And of course, the difference in voltage, corresponding to two different strip chart recorder values, is calculated from the quadratic equation which was fit to the voltage as a function of strip chart recorder value data taken on September 16, and described in table 6.

Table 7 summarizes the reduction of the strip chart calibration and solar irradiance data to yield average values for the insolation during each of the twelve-minute measurements periods, during which the NBS instrument was running. The first four columns of this table are taken from the strip chart recordings. The numbers in the first column are ones to twos, depending upon whether the data on the line on which the number appears is for a period of electrical or a period of solar heating of the receiver. If the data on the line is for a period of solar heating, the computer time at the beginning of the period is recorded in the second column. If the data on the line is for a period of electrical heating, the equivalent irradiance of the electrical power is recorded in the fourth column. In either case, the average value of the strip chart trace for the period is recorded in the third column. The values of ΔE, which correspond to the average values of the strip chart trace for adjacent periods of electrical and radiant heating, are tabulated in the fifth column on the line between the lines on which the data for the adjacent periods of electrical and radiant heating is tabulated. The sum of ΔE and the corresponding equivalent irradiance are tabulated in the sixth column on the same line as ΔE. The average value of the two values so obtained for each period of insolation is tabulated in the seventh column on the line on which the computer time of the beginning of that period of isolation is tabulated.

Table 8 summarizes the relation of the NBS instrument and Ångstrom 210 on September 14.

Tables 9 and 10 are similar to tables 7 and 8, respectively, except they contain the data taken on September 15.

The difference between the means of the ratios, E_{NBS}/E_{210}, obtained on September 14, 1970 and September 15, 1970 is statistically significant and disturbing. None of the other radiometers at Davos showed this behavior relative to Ångstrom 210. But unfortunately this discrepancy was not discovered until after I returned from Davos (since I did not reduce the data in Switzerland once I discovered that the strip chart recorder that I borrowed was nonlinear.) Then it was too late to definitively analyze the discrepancy. However, there is much circumstantial evidence that this discrepancy was caused by a misalignment of ECR #10 relative to the PACRAD in the equitorial mount that supported both detectors. Consequently, I prefer to reject the September 15 data.

In view of the preceding discussion and in view of the new correction factor assigned to ECR #10 in section 5.2, the ratio of the irradiance incident on ECR #10 to that reported by Ångstrom 210 is given by $1.0193 \times 1.0022/1.0035 = 1.0180$ with an estimated limit of error of ± 0.0063.

Table 4: Data Taken on September 11, 1970 to Check the Linearity of the ECR #10. Compare with Table 5.

Time	V mV	E volts	I amps	E/I R ohms	E × I watts	C_f × E × I/V K
1020	.14191	5.0017	.83347	6001.1	.004169	.5488
1023	.14149	5.0013	.83340	6001.1	.004168	.5503
1030	.14159	5.0010	.83347	6000.2	.004168	.5500
1033	.14160	5.0004	.83346	5999.6	.004168	.5499
1036	.14183	5.0035	.83398	5999.5	.004173	.5496
1040	.14183	5.0040	.83392	6000.6	.004173	.5497
1045	.14161	5.0048	.83380	6000.2	.004173	.5505
1048	.14161	5.0045	.83390	6001.3	.004173	.5506
1052	.14144	5.003	.8339	5999.5	.004172	.5510
1055	.14153	5.003	.8339	5999.5	.004172	.5507

R = .55011

St. Dev. of Single Meas. = .12%

St. Dev. of Mean = .04%

Max. Dev. from Mean = .24%

Table 5: Data Taken on September 11, 1970 to Check the Linearity of ECR #10. Compare with Table 4.

Time	V mV	E volts	I amps	E/I R ohms	E × I watts	C_f × E × I/V K
913	.20561	6.0085	1.0066	5969.1	.006048	.5495
925	.20491	6.0102	1.0062	5973.1	.006047	.5514
930	.20515	6.0088	1.0064	5970.6	.006047	.5507
934	.20516	6.0097	1.0062	5972.7	.006047	.5506
937	.20518	6.0092	1.0062	5972.2	.006044	.5504
941	.20497	6.0090	1.0063	5971.3	.006047	.5511
945	.20488	6.0088	1.0063	5971.2	.006047	.5514
950	.20534	6.0090	1.0063	5971.4	.006047	.5501
954	.20523	6.0088	1.0064	5970.6	.006047	.5505
957	.20512	6.0090	1.0063	5971.4	.006047	.5507

K = .55064

St. Dev. of Single Meas. = .11%

St. Dev. of Mean = .03%

Max. Dev. from Mean = .21%

Table 6: The data taken on September 16 to calibrate the span of the strip chart recorder and a least squares fit of the data to $W = D+EC+FC^2$.

N	C(N)[a]	V(N)[b]
1	20.50	175.00
2	30.00	172.00
3	38.00	170.00
4	42.00	169.00
5	49.00	166.00
6	52.50	166.00
7	57.50	164.00
8	57.50	164.00
9	62.00	163.00
10	70.50	161.00
11	71.50	160.00
12	76.50	159.00
13	83.00	158.00
14	83.50	158.00
15	91.00	156.00
16	92.00	155.00

E	F	In Least Squares Fit of
-.341 + 00	.601 - 03	Above Data to $W = D+EC+FC^2$

N	DV(N)[c]	DW(N)[d]
1	.00	.00
2	3.00	2.95
3	5.00	5.36
4	6.00	6.53
5	9.00	8.53
6	9.00	9.51
7	11.00	10.89
8	11.00	10.89
9	12.00	12.10
10	14.00	14.33
11	15.00	14.58
12	16.00	15.84
13	17.00	17.44
14	17.00	17.56
15	19.00	19.33
16	20.00	19.56

a) C(N) = strip chart reading

b) V(N) = microvolts out of differential voltmeter

c) DV(N) = V(1) - V(N) and

d) DW(N) is the prediction of this quantity by the equation

Table 7: Summary of Data Reduction for September 14, 1970.

Type	Time	Chart Reading X(N)	Equiv-Irradiance E_1	ΔE	$E_2 = E_1 + \Delta E$	E_2
1		73.36	93.97			
				0.75	94.72	
2	9:44	68.05				94.73
				0.76	94.74	
1		73.42	93.98			
				1.72	95.70	
2	10:06	61.40				95.85
				2.01	96.00	
1		75.50	93.99			
				2.33	96.32	
2	10:28	59.22				96.57
				-2.05	96.82	
1		45.83	98.87			
				-1.85	97.02	
2	10:50	57.90				97.04
				-1.78	97.07	
1		46.29	98.85			
				-1.93	96.92	
2	11:12	58.94				97.02
				-1.71	97.13	
1		47.72	98.84			
				-1.71	97.13	
2	11:34	58.94				97.20
				-1.59	97.27	
1		48.50	98.86			
				-1.73	97.13	
2	11:56	59.88				97.22
				-1.55	97.30	
1		49.64	98.85			
				-2.02	96.83	
2	12:19	63.04				96.92
				-1.84	97.02	
1		50.77	98.86			
				-2.65	96.21	
2	12:45	68.68				96.30
				-2.48	96.38	
1	extrapo-lated	(51.90)	(98.86)			

(continued)

Table 7 (continued)

Type	Time	Chart Reading X(N)	Equiv-Irradiance E_1	ΔE	$E_2 = E_1 + \Delta E$	E_2
1	extrapo-lated	(62.78)	(88.67)			
				0.11	88.78	
2	14:15	62.06				88.88
				0.30	88.98	
1		64.14	88.68			
				-3.05	85.63	
2	14:37	86.25				85.74
				-2.85	85.84	
1		65.50	88.69			

Table 8: Comparison of Ångstrom 210 and NBS on September 14, 1970.

Time	E_{NBS}	E_{210}	E_{NBS}/E_{210}
9:44	94.73*	92.93†	1.0194
10:06	95.85	94.05	1.0191
10:28	96.57	94.81	1.0186
10:50	97.04	95.18	1.0195
11:12	97.02	95.35	1.0175
11:34	97.20	95.37	1.0192
11:56	97.22	95.14	1.0219
12:19	96.92	94.91	1.0212
12:45	96.30	94.39	1.0202
14:15	88.88	87.18	1.0195
14:37	85.74	84.33	1.0167

Unweighted Mean = 1.0193

Std. Dev. of a Single Meas. = 0.0015

Std. Dev. of the Mean = 0.0004

*Based on last 6 minutes of run

†Based on first, third, and fourth measurement during run

Table 9: Summary of Data Reduction for September 15, 1970.

Type	Time	X(N)	E_1	ΔE	E_2	E_2
1		89.99	83.94			
				2.34	86.28	
2	10:13	72.50				86.24
				-0.79	86.20	
1		66.93	86.99			
				1.80	88.79	
2	10:43	54.70				88.96
				-1.11	89.14	
1		47.50	90.25			
				-2.06	88.19	
2	11:28	61.04				88.14
				1.36	88.09	
1		70.50	86.73			
				-0.56	86.17	
2	11:50	74.48				86.18
				-0.53	86.18	
1		70.68	86.71			

Table 10: Comparison of Ångstrom 210 and NBS on September 15, 1970.

Time	E_{NBS}	E_{210}	E_{NBS}/E_{210}
10:13	86.24	84.96	1.0151
10:43	88.96	87.43	1.0175
11:28	88.14	86.60	1.0178
11:50	86.18	84.82	1.0160

Unweighted Mean = 1.0166

Std. Dev. of a Single Meas. = 0.0013

Std. Dev. of the Mean = 0.0006

6. Conclusion

This report has described the theory of the errors affecting electrically calibrated detectors in considerable detail, and has presented an illustrative example of the application of this theory to the testing and use of a detector to measure solar irradiance during the Third International pyrheliometer comparisons at Davos, Switzerland in September 1970. The main purpose of the theory developed here is to provide insight into the way various sources of error affect this type of detector, and more importantly to allow the design of experiments to accurately measure corrections for each of these sources of errors. This part of the program is pretty well completed. However, most of the experiments described here were the first of this nature that we had ever performed, and it is clear in retrospect how many of them could be improved. Furthermore, the results of these experiments also suggest that the design of the detector could be improved in many ways. This is most evident in the cavity receiver and the aperture holder. The cavity receiver should be redesigned for a specular, high-absorptance coating, and the aperture holder should be redesigned to reduce the effect of case heating. It is estimated that with a considerable expenditure of time and money, the estimated limits of error for this type of detector can be reduced from the 0.6% obtained at Davos to about 0.1%.

The author gratefully acknowledges the valuable assistance of Alfred W. Crigler in the design and construction of the radiometer and the instrumentation used to characterize it.

7. References

[1] Birge, R. T., Phys. Rev. Supplement, 1, 56 (1929).

[2] Coblentz, W. W., Bur. Standards, Bull. 12, 553 (1916).

[3] Müller, C., Zeits. f. Physik, 82, 1 (1933).

[4] Eppley, M., and Karoli, A. R., J. Opt. Soc. Am., 47, 748 (1957).

[5] Stair, R., Schneider, W. E., and Fussell, W. B., Appl. Opt., 6, 101 (1967).

[6] This was the state of affairs in January 1968; however, two measurements of σ have recently been conducted and are in agreement with the value calculated from atomic constants to within the estimated experimental uncertainties, which are on the order of a few tenths of a percent in both cases. See references 11 and 17.

[7] Guild, J., Proc. Roy. Soc. A, 161, 1 (1937).

[8] Gillham, E. J., Proc. Roy. Soc. A, 269, 249 (1962).

[9] Blevin, W. R., and Brown, W. J., Aust. J. Phys., 20, 567 (1967).

[10] Bischoff, K., Optik, 28, 183 (1968).

[11] Kendall, J. M., Sr., and Berdahl, C. M., Appl. Opt., 9, 1082 (1970).

[12] Carslaw, H. S., and Jaeger, J. C., Conduction of Heat in Solids (University Press, Oxford, 1959), 2nd ed., p. 10.

[13] Jakob, M., Heat Transfer, Vol. 1 (John Wiley and Sons, New York, 1962), p. 8.

[14] Mathews, J., and Walker, R. L., Mathematical Methods of Physics (W. A. Benjamin, N.Y., 1965), p. 255.

[15] Watson, G. N., Theory of Bessel Functions (University Press, Cambridge, 1948), 2nd ed., p. 367.

[16] Reference 15, eq. 20, p. 80.

[17] Blevin, W. R., and Brown, W. J., Metrologia, 7, 15 (1971).

[18] Reference 3, p. 18.

[19] Gillham, E. J., Brit. J. Appl. Phys., 4, 151 (1953).

[20] Reference 8, p. 257.

[21] Reference 8, p. 272.

[22] Frohlich, C., Geist, J., Kendall, J., and Marchgraber, R. M., to be published in the Proceedings of the International Solar Energy Society Conference 1971 -- Goddard Space Flight Center, Greenbelt, Md., April 1971.

[23] It is the policy of the National Bureau of Standards to avoid mentioning trade names in publications, whenever possible. However, in this case, the use of a trade name is necessary to the proper identification of the material or instrument. This by no means implies an endorsement by the National Bureau of Standards.

[24] Reference 19, p. 155.

[25] Geist, J. C., and Richmond, J. C., On the Absorptance of Cavity-Type Receivers, Nat. Bur. Stand. (U.S.) Tech. Note 575, 38 pages (July 1971).

[26] I would like to acknowledge the assistance of J. J. Filliben of the Statistical Engineering Section of NBS in the statistical analysis of this data.

[27] Schneider, W. E., Appl. Opt. 9, 1410 (1970).

NBS TECHNICAL PUBLICATIONS

PERIODICALS

JOURNAL OF RESEARCH reports National Bureau of Standards research and development in physics, mathematics, and chemistry. Comprehensive scientific papers give complete details of the work, including laboratory data, experimental procedures, and theoretical and mathematical analyses. Illustrated with photographs, drawings, and charts. Includes listings of other NBS papers as issued.

Published in two sections, available separately:

• Physics and Chemistry

Papers of interest primarily to scientists working in these fields. This section covers a broad range of physical and chemical research, with major emphasis on standards of physical measurement, fundamental constants, and properties of matter. Issued six times a year. Annual subscription: Domestic, $9.50; $2.25 additional for foreign mailing.

• Mathematical Sciences

Studies and compilations designed mainly for the mathematician and theoretical physicist. Topics in mathematical statistics, theory of experiment design, numerical analysis, theoretical physics and chemistry, logical design and programming of computers and computer systems. Short numerical tables. Issued quarterly. Annual subscription: Domestic, $5.00; $1.25 additional for foreign mailing.

TECHNICAL NEWS BULLETIN

The best single source of information concerning the Bureau's measurement, research, developmental, cooperative, and publication activities, this monthly publication is designed for the industry-oriented individual whose daily work involves intimate contact with science and technology—*for engineers, chemists, physicists, research managers, product-development managers, and company executives.* Includes listing of all NBS papers as issued. Annual subscription: Domestic, $3.00; $1.00 additional for foreign mailing.

Bibliographic Subscription Services

The following current-awareness and literature-survey bibliographies are issued periodically by the Bureau: Cryogenic Data Center Current Awareness Service (weekly), Liquefied Natural Gas (quarterly), Superconducting Devices and Materials (quarterly), and Electromagnetic Metrology Current Awareness Service (monthly). Available only from NBS Boulder Laboratories. Ordering and cost information may be obtained from the Program Information Office, National Bureau of Standards, Boulder, Colorado 80302.

NONPERIODICALS

Applied Mathematics Series. Mathematical tables, manuals, and studies.

Building Science Series. Research results, test methods, and performance criteria of building materials, components, systems, and structures.

Handbooks. Recommended codes of engineering and industrial practice (including safety codes) developed in cooperation with interested industries, professional organizations, and regulatory bodies.

Special Publications. Proceedings of NBS conferences, bibliographies, annual reports, wall charts, pamphlets, etc.

Monographs. Major contributions to the technical literature on various subjects related to the Bureau's scientific and technical activities.

National Standard Reference Data Series. NSRDS provides quantitative data on the physical and chemical properties of materials, compiled from the world's literature and critically evaluated.

Product Standards. Provide requirements for sizes, types, quality, and methods for testing various industrial products. These standards are developed cooperatively with interested Government and industry groups and provide the basis for common understanding of product characteristics for both buyers and sellers. Their use is voluntary.

Technical Notes. This series consists of communications and reports (covering both other-agency and NBS-sponsored work) of limited or transitory interest.

Federal Information Processing Standards Publications. This series is the official publication within the Federal Government for information on standards adopted and promulgated under the Public Law 89–306, and Bureau of the Budget Circular A–86 entitled, Standardization of Data Elements and Codes in Data Systems.

Consumer Information Series. Practical information, based on NBS research and experience, covering areas of interest to the consumer. Easily understandable language and illustrations provide useful background knowledge for shopping in today's technological marketplace.

CATALOGS OF NBS PUBLICATIONS

NBS Special Publication 305, Publications of the NBS. 1966-1967. When ordering, include Catalog No. C13.10:305. Price $2.00; 50 cents additional for foreign mailing.

NBS Special Publication 305, Supplement 1, Publications of the NBS, 1968-1969. When ordering, include Catalog No. C13.10:305/Suppl. 1. Price $4.50; $1.25 additional for foreign mailing.

NBS Special Publication 305, Supplement 2, Publications of the NBS, 1970. When ordering, include Catalog No. C13.10:305/Suppl. 2. Price $3.25; 85 cents additional for foreign mailing.

Order NBS publications (except Bibliographic Subscription Services) from: Superintendent of Documents, Government Printing Office, Washington, D.C. 20402.